

Article

## Allometric Scaling and Resource Limitations Model of Tree Heights: Part 1. Model Optimization and Testing over Continental USA

Yuli Shi <sup>1,2,†</sup>, Sungho Choi <sup>2,†,\*</sup>, Xiliang Ni <sup>2,3</sup>, Sangram Ganguly <sup>4</sup>, Gong Zhang <sup>5</sup>, Hieu V. Duong <sup>6</sup>, Michael A. Lefsky <sup>6</sup>, Marc Simard <sup>7</sup>, Sassan S. Saatchi <sup>7</sup>, Shihyan Lee <sup>8</sup>, Wenge Ni-Meister <sup>8</sup>, Shilong Piao <sup>9</sup>, Chunxiang Cao <sup>3</sup>, Ramakrishna R. Nemani <sup>10</sup> and Ranga B. Myneni <sup>2</sup>

<sup>1</sup> School of Remote Sensing, Nanjing University of Information Science and Technology, Nanjing 210044, China; E-Mail: ylshi.nuist@gmail.com

<sup>2</sup> Department of Earth and Environment, Boston University, 675 Commonwealth Avenue, Boston, MA 02215, USA; E-Mail: ranga.myneni@gmail.com

<sup>3</sup> State Key Laboratory of Remote Sensing Sciences, Institute of Remote Sensing Applications, Chinese Academy of Sciences, Beijing 100101, China; E-Mails: nixl@irsa.ac.cn (X.N.); cao413@irsa.ac.cn (C.C.)

<sup>4</sup> Bay Area Environmental Research Institute (BAERI)/NASA Ames Research Center, Moffett Field, CA 94035, USA; E-Mail: sangramganguly@gmail.com

<sup>5</sup> Department of Watershed Science, Utah State University, Logan, UT 84322, USA; E-Mail: gongzhang07@gmail.com

<sup>6</sup> Center for Ecological Analysis of Lidar, Natural Resource Ecology Laboratory, Colorado State University, Fort Collins, CO 80523, USA; E-Mails: dr.hieu.duong@gmail.com (H.D.); lefsky@cnr.colostate.edu (M.L.)

<sup>7</sup> Jet Propulsion Laboratory, California Institute of Technology, 4800 Oak Gove Dr., Pasadena, CA 91109, USA; E-Mails: marc.simard@jpl.nasa.gov (M.S.); saatchi@jpl.nasa.gov (S.S.)

<sup>8</sup> Department of Geography, Hunter College of CUNY, New York, NY 10065, USA; E-Mails: shihyanlee@yahoo.com (S.L.); Wenge.Ni-Meister@hunter.cuny.edu (W.N.)

<sup>9</sup> College of Urban and Environmental Sciences and Sino-French Institute for Earth System Science, Peking University, Beijing 100871, China; E-Mail: slpiao@pku.edu.cn

<sup>10</sup> Biospheric Science Branch, NASA Ames Research Center, Moffett Field, CA 94035, USA; E-Mail: rama.nemani@nasa.gov

† These authors contributed equally to this work.

\* Author to whom correspondence should be addressed; E-Mail: schoi@bu.edu; Tel.: +1-617-353-8846; Fax: +1-617-353-8846.

Received: 12 November 2012; in revised form: 14 January 2013 / Accepted: 15 January 2013 /  
Published: 17 January 2013

---

**Abstract:** A methodology to generate spatially continuous fields of tree heights with an optimized Allometric Scaling and Resource Limitations (ASRL) model is reported in this first of a multi-part series of articles. Model optimization is performed with the Geoscience Laser Altimeter System (GLAS) waveform data. This methodology is demonstrated by mapping tree heights over forested lands in the continental USA (CONUS) at 1 km spatial resolution. The study area is divided into 841 eco-climatic zones based on three forest types, annual total precipitation classes (30 mm intervals) and annual average temperature classes (2 °C intervals). Three model parameters (area of single leaf,  $\alpha$ , exponent for canopy radius,  $\eta$ , and root absorption efficiency,  $\gamma$ ) were selected for optimization, that is, to minimize the difference between actual and potential tree heights in each of the eco-climatic zones over the CONUS. Tree heights predicted by the optimized model were evaluated against GLAS heights using a two-fold cross validation approach ( $R^2 = 0.59$ ; RMSE = 3.31 m). Comparison at the pixel level between GLAS heights (mean = 30.6 m; standard deviation = 10.7) and model predictions (mean = 30.8 m; std. = 8.4) were also performed. Further, the model predictions were compared to existing satellite-based forest height maps. The optimized ASRL model satisfactorily reproduced the pattern of tree heights over the CONUS. Subsequent articles in this series will document further improvements with the ultimate goal of mapping tree heights and forest biomass globally.

**Keywords:** tree height; allometric scaling law; resource limitations; GLAS; model optimization

---

## 1. Introduction

Several recent articles have reported generating spatially continuous maps of forest canopy heights and/or biomass using a combination of remote sensing data, *in-situ* measurements and non-physical/non-physiological or statistical scaling approaches (e.g., [1–8]). Tree height estimation, and potentially biomass, is now possible with altimeter data from terrestrial, airborne, and satellite lidar (e.g., [1–4,9–13]). Lidar waveform data from the Geoscience Laser Altimeter System (GLAS) instrument onboard the Ice, Cloud and land Elevation Satellite (ICESat) have been used to map global and regional forest heights [1,2] and live aboveground biomass [3,4,13]. However, discrete distributions of tree heights retrieved from GLAS data should be extrapolated to generate continuous maps of forest heights or biomass [1,2,4]. This “black-box” type of extrapolation has the obvious limitation that it is often done using non-physical/non-physiological procedures in conjunction with spatially continuous remote sensing and climate data.

Physical/physiological models for mapping tree heights or biomass rely on mechanisms governing plant growth. The Allometric Scaling and Resource Limitations (ASRL) model [14] is one such

physical/physiological model. This predicts local maximum tree heights. The ASRL model integrates allometric scaling laws of trees and energy budgets limited by local resources such as water, air temperature, sunlight, and wind [14]. Some researchers (e.g., [15–18]) however doubt the relevance of plant allometric scaling laws given the high variability observed in actual forests [19,20]. Other studies have demonstrated the applicability of scaling laws for quantifying forest structure and dynamics (e.g., [21,22]) and estimating live biomass in forest stands (e.g., [23,24]). The ASRL model implements the steady-state allometric approach based on the assumption that physiological traits of trees generally follow allometric scaling rules [14]. Nevertheless, the allometric coefficients and scaling exponents of the ASRL model are assumed constant across different eco-climatic zones and forest types of varying age classes. This often results in disparities between measurements and model predictions. Here, a significant progress in mapping tree heights and biomass is possible if the power of allometric scaling laws, local energy budgets and resource limitations can be incorporated with the advancements of remote sensing altimetry (*i.e.*, GLAS data) for scaling purposes.

Generating continuous fields of tree heights and biomass is the larger objective of this multi-part series of articles. In this first article, we focus on how the ASRL model can be used with GLAS data to map actual tree heights over the continental USA (CONUS) at 1 km spatial resolution. The ASRL model is briefly explained in Section 2 together with key equations and parameters. Section 3 includes descriptions of input data for ASRL model and GLAS data preprocessing. Information of the model optimization and evaluation is provided in Section 4 followed by results and discussion (Section 5) and concluding remarks (Section 6). The second paper of this series [25] examines in detail how the same procedures work at a local scale, specifically at several FLUXNET sites. Future articles in the series will consolidate these results and extend them to biomass estimation.

## 2. The ASRL Model

The ASRL model [14] predicts potential maximum tree heights using a combination of allometric scaling laws and energy budgets constrained by local resource limitations, such as water, air temperature, solar radiation, and wind. The model incorporates estimates of parameters related to tree geometry (e.g., canopy radius and leaf area), light (e.g., soil reflectance, leaf absorptivity and deep canopy reflection coefficient), and water flow (e.g., root absorption coefficient, depth of a stomata, and an exponent for metabolism).

In the fundamental premises of the ASRL model, a tree obtains sufficient resources (water and nutrients) to meet its needs for the growth and the availability of local resources limits the maximum potential growth. This is expressed by an inequality equation of basal metabolic rates ( $Q_p \geq Q_e \geq Q_0$ ), where  $Q_p$  is the available flow rate,  $Q_e$  refers to the potential evaporative flow rate, and  $Q_0$  corresponds to the required flow rate of resources in a tree [14].  $Q_0$  is solely determined by allometric scaling rules, while  $Q_p$  and  $Q_e$  are additionally associated with local resources, such as water, air temperature, solar radiation, and wind. The maximum tree growth can be calculated given  $Q_p$  and  $Q_e$ . Key equations of the ASRL model are given in Table 1 [14].

The maximum tree growth varies depending on many factors (e.g., climatic and soil condition, forest types and stand ages), but the ASRL model implements consistent allometric scaling parameters and exponents across different eco-climatic regimes and forest types of varying age classes [14]. In

this study, we test where the ASRL model prediction successes and fails. Our optimization process adjusts several allometric parameters to minimize the difference between actual observations and the model predictions. More details are explained in Section 4.3.

**Table 1.** Key equations of the Allometric Scaling and Resource Limitations (ASRL) model [14]. Underlined variables ( $\alpha$ ,  $\eta$ , and  $\gamma$ ) are selected parameters in the ASRL model optimization, further explained in Section 4.3.

Categories	Variables	Symbols	Key Equations	Sub-Variables
Equations of Basal Metabolic Rates	Available Flow Rate	$Q_p$	$Q_p = \gamma \pi r_{root}^2 P_{inc}$	$\gamma$ = Root Absorption Efficiency; $r_{root}$ = Radial Extent of Root System; $P_{inc}$ = Incoming Precipitation Rate
	Evaporative Flow Rate	$Q_e$	$Q_e = a_f E_{can} \mu_w \rho_w^{-1}$	$a_f$ = Effective Area over the Latent Heat Flux Loss; $E_{can}$ = Evaporative Flux of Canopy; $\mu_w$ = Molar Mass of Water (= $1.80 \times 10^{-2}$ kg·mol <sup>-1</sup> ); $\rho_w$ = Density of Water (= $1.0 \times 10^3$ kg·m <sup>-3</sup> )
	Required Flow Rate	$Q_0$	$Q_0 = \beta_2 h^{\eta_2}$	$\beta_2$ = Proportionality Constant for Metabolism ( $\approx 9.2 \times 10^{-7}$ L·day <sup>-1</sup> ·cm <sup>-<math>\eta_2</math></sup> ); $h$ = tree height; $\eta_2$ = Exponent for Metabolism ( $\approx 2.7$ )
Sub-equations of Evaporative Flow Rate	Effective Area over the Latent Heat Flux Loss	$a_f$	$a_f = 2 a_L \delta_s a_s$	$a_L$ = Total One-sided Area of All Leaves on a Tree; $\delta_s$ = Density of Stomata on a Leaf (=220 stomata·mm <sup>-2</sup> ); $a_s$ = Area of a Single Stomata (=235.1 $\mu\text{m}^2$ )
	Total One-sided Area of All Leaves on a Tree	$a_L$	$a_L = \alpha n^N$	$\alpha$ = Area of Single Leaf; $n$ = Branching Parameter (=2); $N$ = Number of Branching Generations
	Number of Branching Generations	$N$	$N = 2 \ln (r_0/r_N)/\ln n$	$r_0$ = Maximum Stem Radius; $r_N$ = Radius of Terminal Branch (=0.4 mm)
	Evaporative Flux of Canopy	$E_{can}$	Refers to [14]	Equation uses Rate of Absorbed Solar Radiation ( $R_{abs}$ ) along with Canopy Radius ( $r_{can}$ ) and Area of Single Leaf ( $\alpha$ )
Sub-allometric Scaling Equations	Radial Extent of Root System	$r_{root}$	$r_{root} = \beta_3^{1/4} h$	$\beta_3$ = Root to Stem Mass Proportionality ( $\approx 0.423$ )
	Maximum Stem Radius	$r_0$	$r_0 = 0.5 (\beta_2/\beta_1)^{1/\eta_1} h^{\eta_2/\eta_1}$	$\beta_1$ = Proportionality Constant for Metabolism (=0.257 L·day <sup>-1</sup> ·cm <sup>-<math>\eta_1</math></sup> ); $\eta_1$ = Exponent for Metabolism (=1.8)
	Canopy Radius	$r_{can}$	$r_{can} = \beta_5 h^\eta$	$\beta_5$ = Proportionality Constant for Canopy Radius (=35.24 cm·m <sup>-<math>\eta</math></sup> ); $\eta$ = Exponent for Canopy Radius

### 3. Data

#### 3.1. Input Data for the ASRL Model

The key input climatic variables include annual total precipitation, annual average temperature, annual incoming solar radiation, annual average wind speed and annual average relative humidity.

Additionally, two categories of ancillary input data are needed: (a) Digital Elevation (DEM) and Leaf Area Index (LAI) for initializing the ASRL model and (b) land cover and tree cover for delineating forested lands.

Table 2 lists input data (climate data and ancillary inputs) required for the ASRL model. Finer gridded data (e.g., 30 m or 250 m) were resampled to 1 km resolution in this study using the majority principle for categorical values and cubic convolution for numerical values [26]. Wind speed data at 32 km resolution were spatially interpolated to 1 km resolution using an Inversed Distance Weighting (IDW) method [27].

**Table 2.** Climatic and other ancillary variables used for ASRL model simulations.

Types	Required Input Variables	Units	Temporal Range	Spatial Resolution	Used Data Sets
Climatic Variables	Annual Total Precipitation	mm	1980–1997	1 km	DAYMET model [28]—Annual Average Relative Humidity (%) was computed by the formula provided by World Meteorological Organization (WMO) [29]
	Annual Average Temperature	°C	1980–1997	1 km	
	Annual Incoming Solar Radiation	W/m <sup>2</sup>	1980–1997	1 km	
	Annual Average Vapor Pressure	hPa	1980–1997	1 km	
	Annual Average Wind Speed	m/s	2000–2008	32 km	
Ancillary Variables I	Digital Elevation (DEM)	m	2009	30 m	National Elevation Dataset (NED) [31]
	Growing Season Average Leaf Area Index (LAI)	N/A	2003–2006 Jun–Sep	1 km	Post-processed Moderate Resolution Imaging Spectroradiometer (MODIS) LAI products [32]
Ancillary Variables II	Land cover	N/A	2006	30 m	National Land Cover Database (NLCD) [33]
	Percentage of Tree Cover	%	2005	250 m	MODIS Vegetation Continuous Fields (VCF) Collection 5 [34]

### 3.1.1. Climate Data

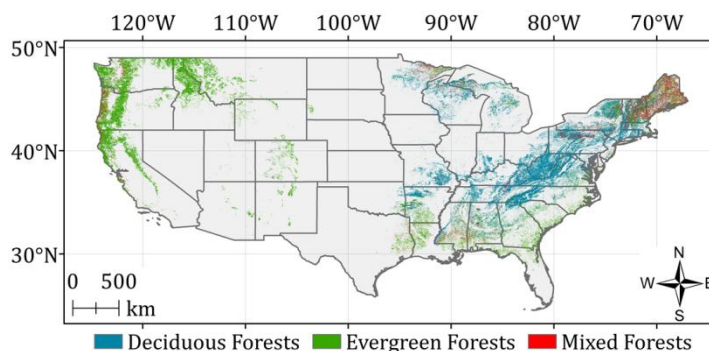
The ASRL model was mostly driven by climatic variables derived from the DAYMET model [28]. The DAYMET model uses daily weather observations (1980–1997) to produce wall-to-wall climate grids of annual total precipitation, annual average temperature, annual incoming solar radiation and annual average vapor pressure over CONUS. Annual relative humidity, an input parameter of the ASRL model, was derived from annual average temperature and annual vapor pressure using functional relationships provided by the World Meteorological Organization (WMO) [29] (Section S1.1 of Supplementary Information). Wind speed was derived from the North American Regional Reanalysis (NARR) data [30]. The NARR provides monthly mean values from 1979 till present at a spatial resolution of 0.3-degree (~32 km). Monthly mean values from years 2000 to 2008 were averaged to obtain annual average values and used as input to the ASRL model.

### 3.1.2. Ancillary Data

The first set of ancillary data (DEM and LAI) is used for the initial ASRL predictions of potential tree heights. The growing season (June to September) average LAI data were calculated from a refined version of the standard Moderate Resolution Imaging Spectroradiometer (MODIS) LAI products (1 km grids) for the time period from 2003 to 2006 [32] (Section S1.2).

The second set of ancillary data is required during the ASRL model prediction and the parametric optimization to identify forested lands. The model simulations were conducted on spatial regions categorized into three forest classes—deciduous, evergreen, and mixed forests—each with percent tree cover  $\geq 50$  percent based on the MODIS Vegetation Continuous Field (VCF) product (Figure 1).

**Figure 1.** Forested lands (1 km spatial resolution) over the continental USA (CONUS) based on the National Land Cover Database (NLCD) 2006 land cover. Three forest types—deciduous, evergreen, and mixed forests—with percent tree cover  $\geq 50\%$  were considered in this study.



### 3.2. GLAS Tree Heights

The GLAS laser altimetry data provide information related to land elevation and vegetation height at a spatial resolution of  $\sim 70$  m (ellipsoidal footprints) and at  $\sim 170$  m spaced intervals [35,36]. The latest release (Release-33) of the standard GLAS product corresponding to the GLAS Level-2 Land Surface Altimetry (GLA14; L2 Land Surface Altimetry) for the period 2003 to 2006 was obtained from the National Snow and Ice Data Center (NSIDC) for this study. The GLA14 product was used to estimate forest canopy heights within each footprint (e.g., [1,3]) using geolocation information and waveform parameters, such as signal beginning and echo energy peaks [37]. There are notable heterogeneities in the dimension and shape of the individual GLAS footprints. The GLAS instrument was designed to have a fixed footprint size, but the dimensions of footprints are significantly changed depending on the laser periods (e.g., orbits and spans of campaigns) [38]. To simplify, we assumed that all GLAS footprints have a circular diameter of 70 m [39]. Data from May to October of each year were used, as these come from the growing season and correspond to the MODIS LAI product.

GLAS waveform data are affected by three degrading factors: (a) atmospheric forward scattering and signal saturation, (b) background noise (low cloud) and (c) slope gradient effects. Additionally, GLAS footprints over non-forest and/or bare ground must be filtered from analysis. Five screening steps were applied to remove invalid GLAS waveform data prior to retrieval of tree heights (Table 3).

Note that we removed any remaining outliers using two standard deviations from the mean of GLAS tree heights ( $5 \text{ m} < H_{GLAS} \leq 100 \text{ m}$ ) in this analysis. Final valid GLAS footprints were intersected with the pixels ( $=1 \text{ km}$ ) over forested lands. We averaged tree heights derived from the GLAS footprints falling in a pixel. This generates a raster distribution of GLAS heights (Figure S1).

**Table 3.** Five screening steps to remove invalid Geoscience Laser Altimeter System (GLAS) footprints over the CONUS. Final valid GLAS footprints are 126693 in this study.

Screening Steps	Description	Number of Valid GLAS Footprints	References
1. Atmospheric Forward Scattering and Signal Saturation Filter	- Cloud-free and saturation-free GLAS waveform data; - Internal flag of GLAS data—"FRir_qaFlag = 15" and "satNdx = 0"	1,822,739	[3]
2. NLCD and VCF Filters	- GLAS footprints over forested lands; - Geolocation of NLCD and VCF pixels (pixels nearest to the center of a GLAS footprint); - Deciduous, evergreen, and mixed forests with greater than 50% of the tree cover	1,659,061	-
3. Background Noise Level (Low Cloud) Correction Filter	- No background noise level in GLAS waveform data; - Absolute difference ( $\leq 50 \text{ m}$ ) between the NED DEM and the internal elevation ("i_elev") of GLAS waveform data	161,533	[36,40]
4. Slope Gradient Correction Filter	- GLAS footprint over non- high topographic condition; - Slope value $< 20^\circ$ of the nearest pixel from GLAS data; - Additionally correction of the potential bias (= footprint size $\times \tan(\text{slope})$ )	129,705	[25,40,41]
5. Removal of Remaining Outliers	- Using two standard deviations from the mean of GLAS tree heights ( $5 \text{ m} < H_{GLAS} \leq 100 \text{ m}$ )	<u>126,693</u> (Final)	-

There are two approaches of retrieving tree heights from GLAS waveform data [40]: (a) the "statistical analysis for examining full GLAS waveform extents" [41–44] and (b) the "decomposition of GLAS waveforms into multiple Gaussian distribution curves" [1,3,6,40,45–47]. We considered only the second approach in this study.

We used two standard altimetry variables of GLA14 product (signal begin range increment, *SigEndOff*; centroid range increment for the last Gaussian Peak, *gpCntRngOff* 1). Theoretically, *gpCntRngOff* 1 is assumed to represent the ground level elevation within a GLAS field-of-view, while *SigBegOff* refers to the highest point of a surface. Amongst five possible GLAS height metrics representative of tree heights [25], we used the best metric that closely resembled field-measured and Laser Vegetation Imaging Sensor tree heights ( $R^2 = 0.70$ ; RMSE = 4.42 m; [25]): that is, "*SigBegOff* – *gpCntRngOff* 1" with correction of the potential bias [40] (Equation (1)).

$$H_{GLAS} = (SigBegOff - gpCntRngOff) - \frac{d \times \tan \theta}{2} \quad (1)$$

Here, *SigBegOff* is the signal begin range increment and *gpCntRngOff* 1 refers to the last peak of Gaussian of GLAS waveform, *d* is the footprint diameter of GLAS data ( $\sim 70 \text{ m}$ ) and  $\theta$  is the slope value nearest to the geolocation of GLAS footprint center.

## 4. Methods

### 4.1. Defining Climatic Zones

The forested area in the CONUS was categorized into 841 climatic zones based on three forest types, annual total precipitation (30 mm intervals) and annual average temperature (2 °C intervals). An empirical orthogonal panel [48,49] was used to identify the pattern of these two climatic variables (horizontal axis—annual total precipitation and vertical axis—annual average temperature), and to associate forested grids to climatic zones (Figure S2; Table 4).

The reasons for defining climatic zones are twofold: First, a direct comparison of GLAS heights, which represent actual tree heights, with potential tree heights predicted by the ASRL model is not valid. Second, optimization of the ASRL model for every forested pixel (over 1.3 million pixels) is not computationally practical. Thus, the optimization was performed at the climatic zone level for each of the three forest types.

**Table 4.** Definition of climatic zones for grouping pixels within a forested area. Three forest types with fixed ranges of annual total precipitation (30 mm intervals) and annual average temperature (2 °C intervals) yield a total of 5805 segments ( $3 \times 129 \times 15$ ). Of these, only 841 climatic zones have at least one GLAS observation.

Forest Types (Deciduous, Evergreen, and Mixed Forests)	Annual Total Precipitation (mm)			Annual Average Temperature (°C)			Climatic Zones Effective
	Lower Limits	Upper Limits	Intervals	Lower Limits	Upper Limits	Intervals	
3	300	4,170	30	−5	25	2	841

### 4.2. Initial ASRL Model Prediction of Potential Tree Heights

ASRL model simulations were performed over forested areas (Section 3.1.2). The ASRL model predicts potential tree heights at 1 km spatial resolution using input climatic and ancillary variables (Section 3.1). There are notable disparities between model predicted tree heights and actual observations—the reason being that the ASRL model includes constant scaling exponents and parameters across different climatic regimes and forest types.

### 4.3. Optimization of the ASRL Model

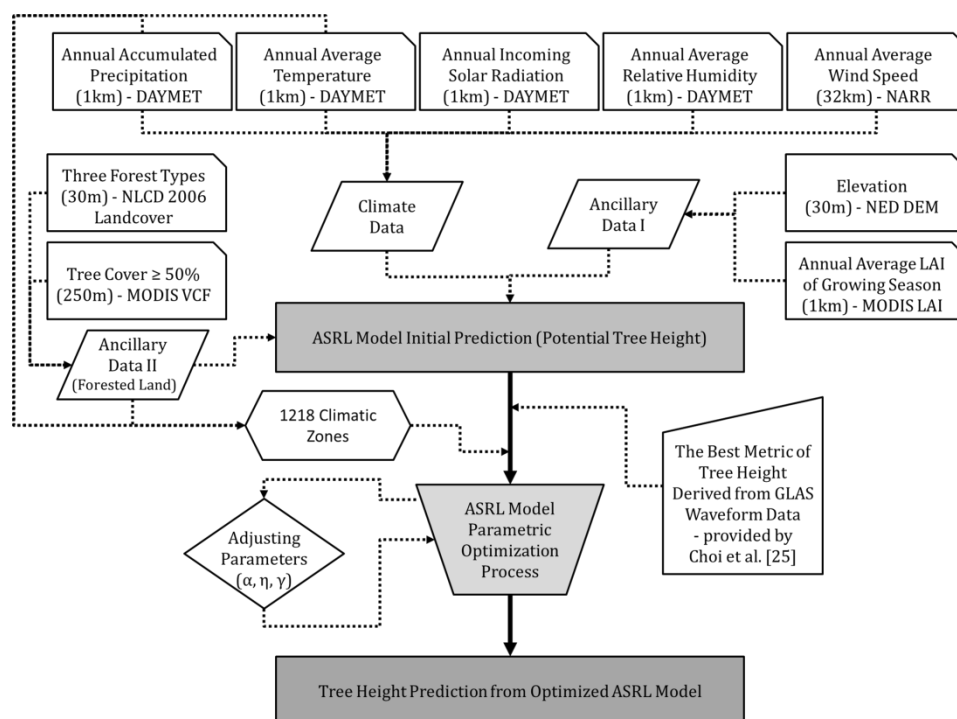
Optimization of the ASRL model was designed to simultaneously adjust multiple scaling parameters. This optimization was aimed to minimize the difference between actual tree heights derived from GLAS data and tree heights predicted by the ASRL model (Figure 2). The underlying theoretical framework is based on Powell's optimization methodology [50] that results in finding the minima of a multidimensional function. This algorithm is efficient for generating the convergence of a function due to (a) its bi-directional search algorithm over the vector of multi-variables and (b) nonessential calculation of derivatives for each variable [50]. A function involving three variables (merit function as in Equation (2)) was formulated and implemented based on Press *et al.* [51] and Kuusk and Nilson [52].

Three parameters of the ASRL model—area of single leaf ( $\alpha$ ), exponent for canopy radius ( $\eta$ ) and root absorption efficiency ( $\gamma$ )—were selected for optimization. Initial values of these three parameters ( $\alpha$ ,  $\eta$ , and  $\gamma$ ) were set to 13 cm<sup>2</sup>, 1.14, and 0.33, respectively. These values are comparable to the representative values (averages) from the TRY database [53] and also based on Kempes *et al.* [14]. Although there are other physiological traits available from the TRY database [54], this study was limited to optimization of these three parameters.

The collection of solar radiation for plant growth is associated with the coefficient for canopy transmissions. Here,  $\alpha$  produces the total leaf area based on the branching generation theory [55]. In the ASRL model, the canopy-level budget is collected from the energy budget in a single leaf based on the allometric geometry of canopy [14]. The value  $\eta$  controls the scaling of canopy radius with tree height, which is related to the rate of absorbed solar radiation. Lastly,  $\gamma$  determines the available flow rate given the incoming rate of precipitation within the root capture area. The tallest tree takes  $\gamma$  (=1/3) on average and local  $\gamma$  varies across different soil type and hydrology [14].

Kempes *et al.* [14] have performed the sensitivity tests of several allometric scaling exponents, and  $\eta$  showed the second least sensitivity. The value  $\gamma$  was tested in the optimization procedures of Kempes *et al.* [14], generating clear improvement of the model predictions. In this study,  $\alpha$  was additionally selected for optimization due to (a) its strong relationship to net absorbed radiation, sensible and latent heat fluxes (e.g., [56]) and (b) considerable variability of  $\alpha$  across different climatic zones and forest types [57,58].

**Figure 2.** Diagram showing the optimization of the ASRL model. The model predicts potential tree heights (initial prediction) based on input climatic and ancillary variables. Three allometric scaling parameters (area of single leaf,  $\alpha$ , exponent for canopy radius,  $\eta$  and root absorption efficiency,  $\gamma$ ) are adjusted in the optimization process to minimize the difference between GLAS tree heights and ASRL modeled tree heights. This optimization process is done separately for each of the climatic zones.



The optimization process stops the iterative adjustment of the three parameters when it finds the maximum likelihood estimates of each parameter that result in minimizing the merit function. To reach an optimal solution, we implemented variable ranges (lower and upper boundaries as in the TRY database) for each of the input parameters such that  $1 \text{ cm}^2 \leq \alpha < 100 \text{ cm}^2$ ,  $0.8 \leq \eta < 1.5$ , and  $0.1 \leq \gamma < 0.8$ . Equation (2) shows the merit function,

$$J(p_1, p_2, p_3) = \sum_{k=1}^3 \left[ (p_k - p_{kb})^4 w_k^2 + \frac{(p_k - p_{k0})^2}{\Delta_{p_k}^2} \right] + \sum_{i=1}^N \frac{(H_{ASRL,i} - H_{GLAS,i})^2}{\Delta_H^2} \quad (2)$$

Here  $p_k$  is the selected ASRL model parameter ( $k$ ; 1 = area of single leaf, 2 = exponent for canopy radius, and 3 = root absorption efficiency),  $p_{k0}$  refers to the initial values of each parameter in the original ASRL model,  $p_{kb}$  refers to the boundary limits ((lower limit + upper limit)/2) for each parameter,  $\Delta_{pk}$  is the standard deviation associated with each parameter with respect to initial values,  $w_k$  is a scalar weight ( $w_k = 0$  when  $p_k \in [p_{k\_lower-limit}, p_{k\_upper-limit}]$ , otherwise  $w_k = 10$ ),  $N$  is the total number of comparison sets ( $i$ ) for GLAS heights ( $H_{GLAS}$ ) and ASRL model predictions ( $H_{ASRL}$ ) with given parameter values for each climatic zone and  $\Delta_H$  is the standard deviation associated with  $H_{GLAS}$  and  $H_{ASRL}$ . The iterative adjustment process continues until it finds the minimum of the function  $J(p_1, p_2, p_3)$  for each of the climatic zones.

A noteworthy limitation of this optimization exercise is that forest stand ages are not directly involved in the optimization process. Tree heights and growth rates vary depending on forest types and sites due to different growing conditions. Those are clearly related to forest stand ages [59–61]. When a tree ages, its height increases along with decline in the rate of its vertical growth over time—young forest stands (~10 years) grow in the southeastern region, while old forest stands (~900 years) inhabit the western coasts in CONUS [62]. However, it does not necessarily mean that our methodology neglects forest stand ages in tree height estimations. GLAS waveform data indirectly brings age information of forests into the ASRL model to find appropriate scaling parameters, as actual heights are associated with forest stand ages.

Performance of the ASRL model was tested by comparing GLAS tree heights and model predicted heights (with and without optimization). The goal was to show the efficacy of the optimization process. We calculated  $R^2$  and root-mean-square-error (RMSE) from relationships between GLAS tree heights and model predicted heights in each climatic zone (Equation (3)).

$$RMSE_{ASRL} = \sqrt{\frac{\sum_{i=1}^n (\bar{H}_{ASRL,i} - \bar{H}_{GLAS,i})^2}{n}} \quad (3)$$

Here  $\bar{H}_{ASRL}$  is the mean of tree heights from ASRL model predictions (with and without optimization) in each climatic zone,  $\bar{H}_{GLAS}$  is the mean of tree heights derived from GLAS waveform data in each climatic zone, and  $i$  refers to the number of climatic zones ( $n = 841$ ).

The training datasets of GLAS used in model optimization are identical to the test datasets of GLAS used for evaluation [63]—this was first done to assess whether the optimization scheme was correctly implemented or not. It was not meant to establish validity of the optimized ASRL model. The actual evaluation of the optimized ASRL model was performed as detailed below.

#### 4.4. Evaluation of the Optimized ASRL Model Results

The prediction of the optimized ASRL model was evaluated in two parts: (a) two-fold cross validation approach and (b) two inter-comparisons of optimized ASRL model prediction ( $H_{opt\ ASRL}$ ) with forest canopy heights produced by Simard *et al.* [1] ( $H_{Simard}$ ) and Lefsky [2] ( $H_{Lefsky}$ ). Each evaluation performs inter-comparisons at the climatic zone level and at the pixel level.

##### 4.4.1. Two-Fold Cross Validation

A two-fold cross validation approach was performed: That is, we randomly divided the original sample input data into two sets of training and test data. The first half of the GLAS tree heights was used as a training data to optimize the ASRL model in each climatic zone. The test data was generated by averaging the remaining half of the GLAS tree heights in each climatic zone and used for model evaluation purposes (Equation (4)). In addition, pixel level comparisons were performed to evaluate model prediction errors ( $H_{opt\ ASRL\ training} - H_{GLAS\ test}$ ). We selected spatially corresponding tree height values (the nearest pixels) in pixel level comparisons.

$$RMSE_{ASRL\ two\ fold\ cross\ valid.} = \sqrt{\frac{\sum_{i=1}^n (\bar{H}_{opt\ ASRL\ training\ i} - \bar{H}_{GLAS\ test\ i})^2}{n}} \quad (4)$$

Here  $H_{opt\ ASRL\ training}$  is the predicted height by the optimized ASRL model using the first set of GLAS training data for each climatic zone,  $H_{GLAS\ test}$  is the mean of tree heights computed from the second set of GLAS test data in each climatic zone, and  $i$  refers to the number of climatic zones ( $n = 245$ ). In these climatic zones, the number of pixels with GLAS tree height data was more than 20.

##### 4.4.2. Inter-comparison with Other Forest Height Maps

The optimized model evaluations were additionally performed by comparing model predicted heights with  $H_{Simard}$  and  $H_{Lefsky}$ . Linear regression analysis between model predicted tree heights and the two maps was performed for each of the climatic zones. Pixel level evaluations used differences in histograms that were differentiated by forest types: deciduous, evergreen, and mixed forests. Some caveats are in order regarding these inter-comparisons: (a) the metric of forest height map in Lefsky [2] is Lorey's height—basal area weighted mean height, while Simard *et al.* [1] and our research used maximum canopy height, (b) the forest height map of Simard *et al.* [1] does not allow tree height values >40 m, (c) both Simard *et al.* and Lefsky differ in their definition of forested lands, and (d) final products of Simard *et al.* [1] and Lefsky [2] are at different spatial resolution (1 km and 500 m, respectively) and different map projection.

To facilitate inter-comparison with  $H_{Simard}$ , we resampled and reprojected the forest height map of Simard *et al.* [1] to match our map of model predicted tree heights. The comparison was then performed over pixels that spatially corresponded to our definition of forested lands.

On the other hand, a direct comparison between Lefsky [2]'s forest heights and our results was not feasible for the reason of different measures (Lorey's height *versus* maximum tree heights). Therefore, we used Lefsky [2]'s input GLAS heights data, rather than the final product of Lefsky [2]. For the inter-comparison, we averaged Lefsky's GLAS heights falling in a pixel (=1 km) of the forest lands.

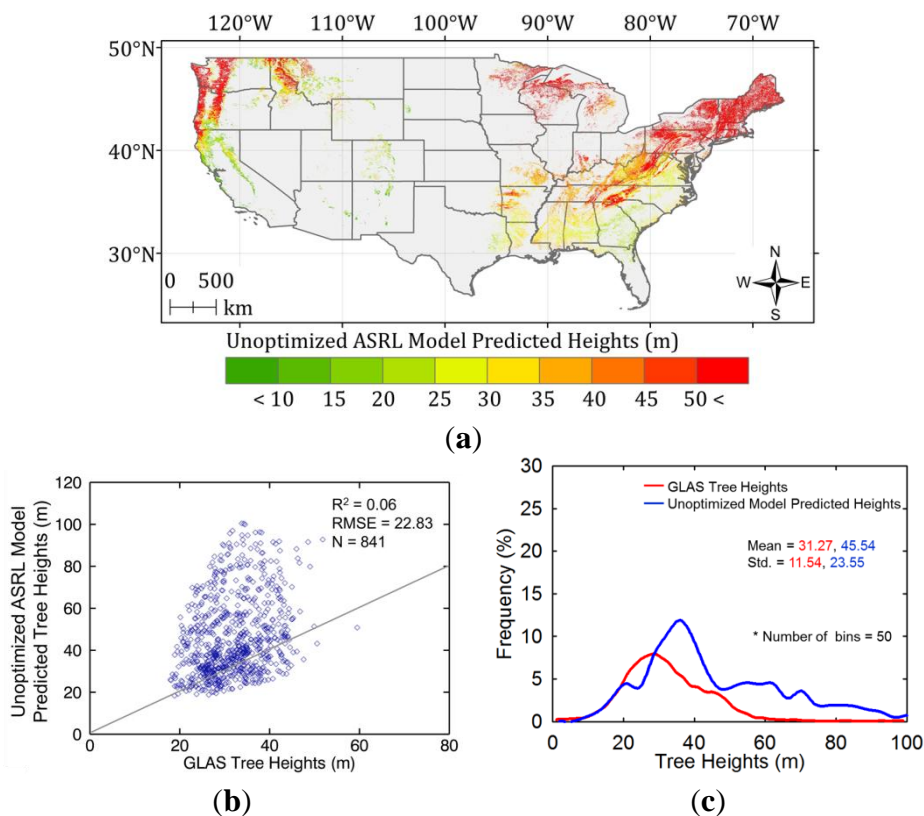
There are certain limitations of our analysis in the ASRL model predictions and evaluations: (a) up- and down-scaling approaches of resampling may cause potential errors due to the aggregation of heterogeneity in finer grids and the neglect of discontinuity in coarser datasets [64,65] and (b) the reprojection possibly results in certain modification of true pixel values [66].

### 5. Results and Discussion

#### 5.1. Initial ASRL Model Predictions of Potential Tree Heights

A continuous map of potential tree heights ( $H_{potential\ ASRL}$ ) was generated with the unoptimized ASRL model at 1 km resolution (Figure 3(a)). Maximum potential tree heights were greater than 50 m in both the Northeastern Appalachian and Pacific Northwestern forest corridors. The model predicted lower values of potential tree heights ( $\leq 35$  m) in the Southeast.

**Figure 3.** (a) Map of potential tree heights predicted by the unoptimized ASRL model for the CONUS at 1 km resolution. (b) Comparison between GLAS tree heights and unoptimized model predictions in each of the climatic zones. (c) Histograms showing pixel level comparison between GLAS and potential tree heights. Number of bins of histograms is 50. Frequencies have been normalized by total grids (frequency %).



We noted discrepancies between model predictions and GLAS tree heights ( $H_{GLAS}$ ; actual tree height; Figure S1). A low correlation was observed (Figure 3(b)) in each climatic zone ( $R^2 = 0.06$ ;  $RMSE = 22.8$  m). In addition, there was significant skewness in the histograms of actual (mean = 31.3 m; standard deviation = 11.5) and potential (mean = 45.5 m; std. = 23.6) tree heights at the pixel level (Figure 3(c)). Tree heights were overestimated especially in the northeastern forests as compared to

$H_{GLAS}$  (Figure S3(a)). A plausible reason could be that the ASRL model does not accurately reflect the spatial/temporal dynamics in the estimation of internal flow balances (metabolic flow requirement, available flow, and evaporative flow) across different eco-climatic regimes and forest types [14].

5.2. Optimized ASRL Model Predictions

The optimized model was then used to generate a spatially continuous map of tree heights ( $H_{opt ASRL}$ ; Figure 4(a)). We noted a significant improvement in predictions of tree heights both at the climatic zone level (Figure 4(b)) and individual pixel level (Figure 4(c); Figure S3(b)): (a) the RMSE decreased from 22.8 m (without optimization) to 3.1 m (after optimization) with an increase in  $R^2$  from 0.06 to 0.8 ( $P < 0.01$ ); (b) the histograms show a better agreement between distributions of GLAS tree heights (mean = 31.3 m; std. = 11.5) and the optimized model predictions (mean = 30.4 m; std. = 8.5); and (c) relatively smaller model prediction errors over the Northeastern Appalachian and Pacific Northwestern forest corridors as compared to the unoptimized ASRL model predictions.

**Figure 4.** (a) Spatially continuous map of tree heights predicted by the optimized ASRL model at 1 km spatial resolution. (b) Comparison between GLAS tree heights and the optimized ASRL model predictions in each climatic zone. (c) Histograms at pixel level showing the degree of agreement between GLAS tree heights and the optimized ASRL model predictions. Number of bins of histograms is 50. Frequencies have been normalized by total grids (frequency %).

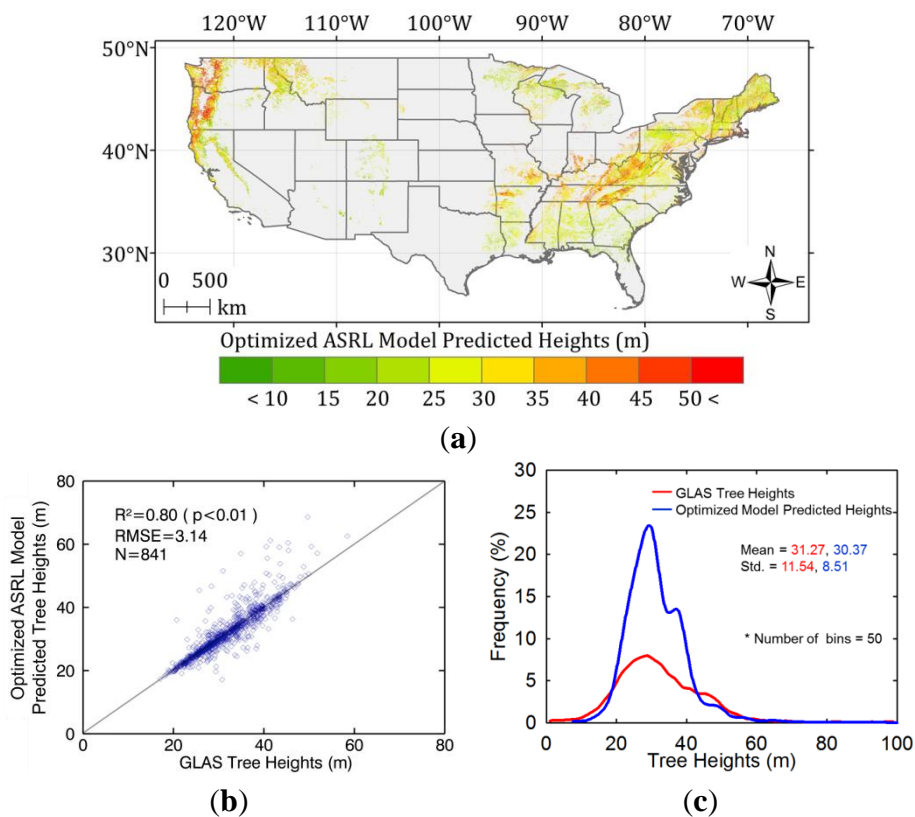
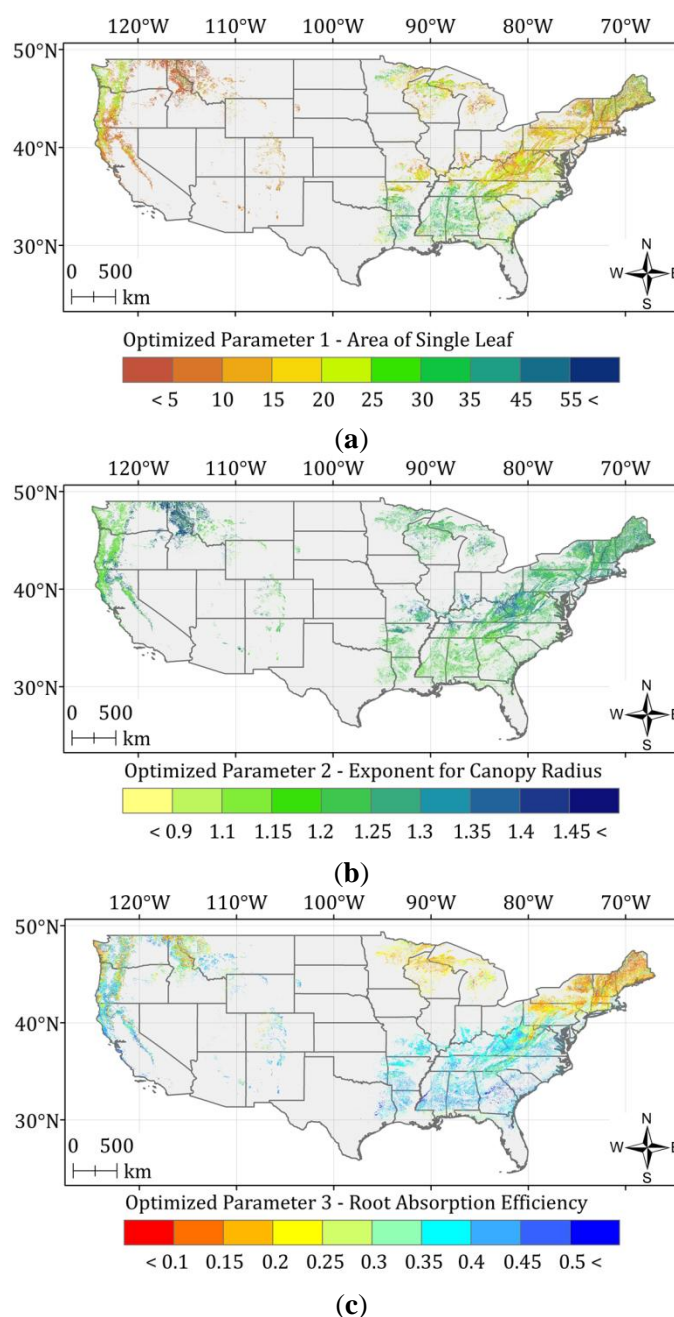


Figure S4 shows that the ASRL model prediction errors at the individual pixel level decreased from 15.10 m ( $H_{GLAS} - H_{potential ASRL}$ ) to  $-0.80$  m ( $H_{GLAS} - H_{opt ASRL}$ ). However, the optimized ASRL model

poorly predicted tree heights over complex terrains (e.g., ~20 m underestimation for the redwood stands in the Pacific Northwestern mountains of California and Oregon; Figure S3b). Other GLAS-based models also reported relatively large prediction errors in the estimation of tree heights [1] and biomass [3] in these forests. Interpolation of annual precipitation (e.g., [67]) and temperature (e.g., [68]) may have produced large uncertainties in climatic variables that are sensitive to topographic features. Note that these are critical inputs to the ASRL model. Other plausible reasons for this discrepancy may be: (a) GLAS undersampling for some of the climatic zones (Figure S5) that resulted in fewer comparison sets in the merit function (Equation (2)) and (b) topographic influence on GLAS waveform data which could not perfectly be rectified by our slope gradient filter (Table 3).

**Figure 5.** Spatial distribution of the three parameters selected for model optimization. (a) Area of single leaf, (b) Exponent for canopy radius and (c) Root absorption efficiency.



The optimized parameters are shown in Figure 5. There are notable changes in the optimal area of single leaf (initial value  $\alpha$ : 13.0 cm<sup>2</sup>) that ranged from 1.5 cm<sup>2</sup> to 90.0 cm<sup>2</sup>. The root absorption efficiency (initial value  $\gamma$ : 0.33) converged to a relatively narrower range of values (from 0.05 to 0.65), while ~80% of the optimized exponent for canopy radius ( $\eta$ ) fell within the range of  $\pm 10\%$  of its initial value (1.14). Kempes *et al.* [14] have also reported a stable median relative error against the percent change of a single scaling parameter (*i.e.*,  $\eta$ ).

The area of single leaf of deciduous forests (mean  $\alpha = 19.3$  cm<sup>2</sup>) was higher than that of evergreen forests (mean  $\alpha = 9.1$  cm<sup>2</sup>). The original ASRL model precludes inclusion of forest types. The optimization process allows combining allometric scaling laws with features that are representative of specific forest types. Optimized  $\alpha$  values are well correlated with the variability in forest types, annual total precipitation and annual average temperature in each climatic zone. Warm (annual average temperature = ~15 °C) and wet (annual total precipitation  $\geq$  ~1,500 mm) regions displayed a larger value of  $\alpha$  for both deciduous and evergreen forests. In cold regions (annual average temperature = ~5 °C), the optimized value of  $\alpha$  for evergreen forests increased with annual total precipitation. These results are supported by other studies that examined relationships between leaf traits and environmental conditions [69–71].

Similar trends in the optimized  $\gamma$  values were observed in warm and wet regions. However, evergreen forests generally showed higher optimized  $\gamma$  values compared to deciduous forests in relatively dry regions. Water availability is spatially heterogeneous for an individual species within a location [72]. For example, evergreen and deciduous plants in dry regions have different root systems and water use efficiencies (evergreen > deciduous as in [73,74]). Kempes *et al.* [14] have demonstrated an improvement of the ASRL model based on optimization of  $\gamma$  that generated a lower variance in the model error.

### 5.3. Evaluation of the Optimized ASRL Model

#### 5.3.1. Two-Fold Cross Validation Approach

Figure 6(a) shows the two-fold cross validation comparison ( $R^2 = 0.59$ ; RMSE = 3.31 m;  $P < 0.01$ ). Histograms comparing the test GLAS heights (mean = 30.8 m; std. = 10.7) and tree heights predicted by the optimized model (mean = 30.6 m; std. = 8.4) show considerable similarity (Figure 6(b)), even though it gives relatively less correlations than using all of valid GLAS tree heights. The satisfactorily low prediction errors (mean = -0.61 m; std. = 12.91) are shown in Figure 6(c). We achieved the stability of the optimized model predictions from the two-fold cross validation.

#### 5.3.2. Inter-comparison with Other Forest Height Maps

Forest height maps from Simard *et al.* [1] and our study portray similar patterns of tree heights over the CONUS: (a) taller trees (> 40 m) in the Pacific Northwestern forests of California and Oregon, (b) relatively medium-to-tall trees (30 to 40 m) in the northeastern forested regions, and (c) smaller trees (~20 to 30 m) along the Great Lake and the Mississippi River basin. It should be noted that the regression tree procedure described in Simard *et al.* [1] is based on the GLAS altimetry variables of the

Gaussian decomposition (signal beginning, signal end, and last Gaussian peak). Simard *et al.* [1] also included a similar set of environmental layers related to elevation, temperature, and precipitation.

**Figure 6.** A two-fold cross validation approach showing comparisons between test GLAS tree heights and the optimized ASRL model predictions using training GLAS tree heights. We randomly divided the GLAS height data into two equal sets of training and test data: (a) Scatter plot of tree heights for each of the climatic zones. A total of 245 climatic zones were considered in this comparison (available number of GLAS tree height data  $\geq 20$  in each climatic zone). (b) Pixel level histogram comparison. (c) Optimized ASRL model prediction errors ( $H_{opt\ ASRL\ training} - H_{GLAS\ test}$ ) from pixel level comparison. Number of bins of histograms is 50. Frequencies have been normalized by total grids (frequency %).

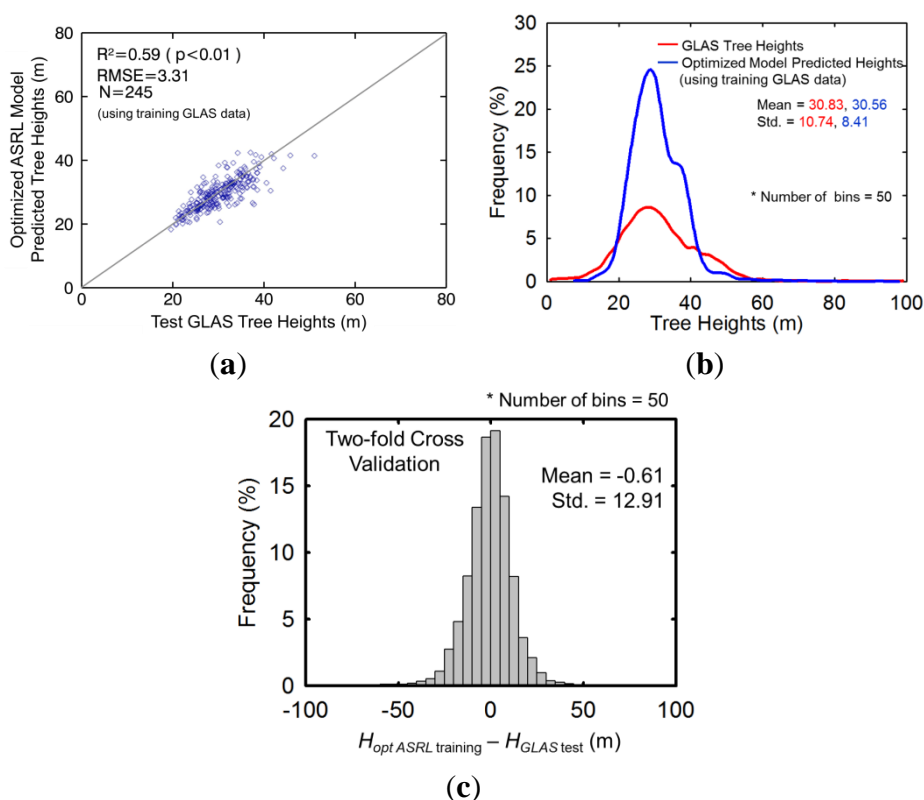
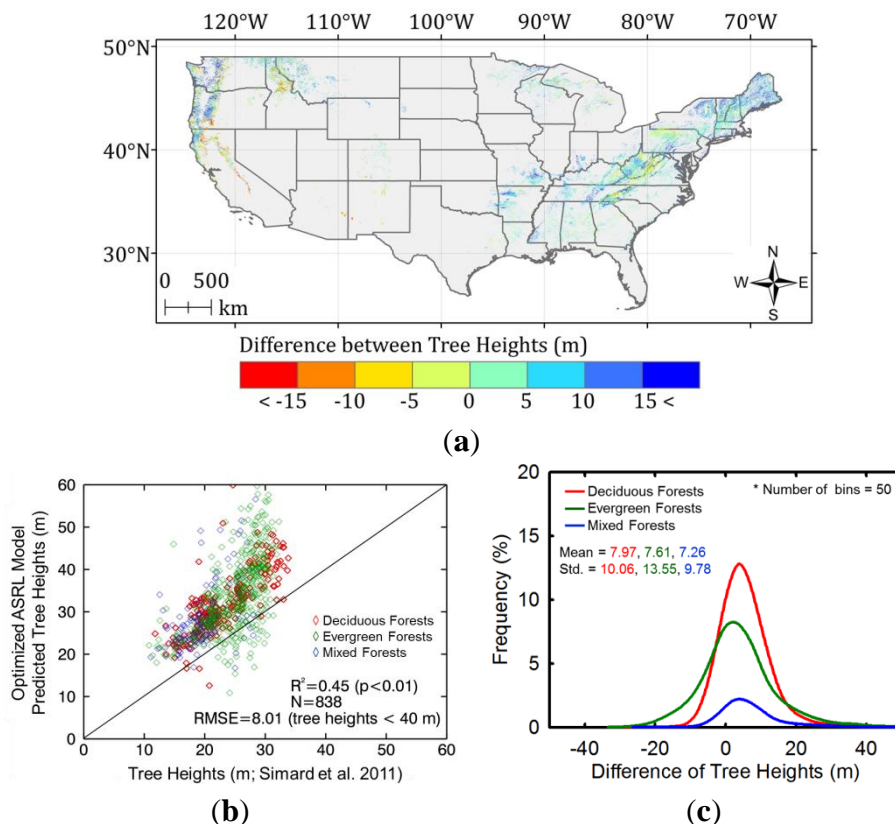
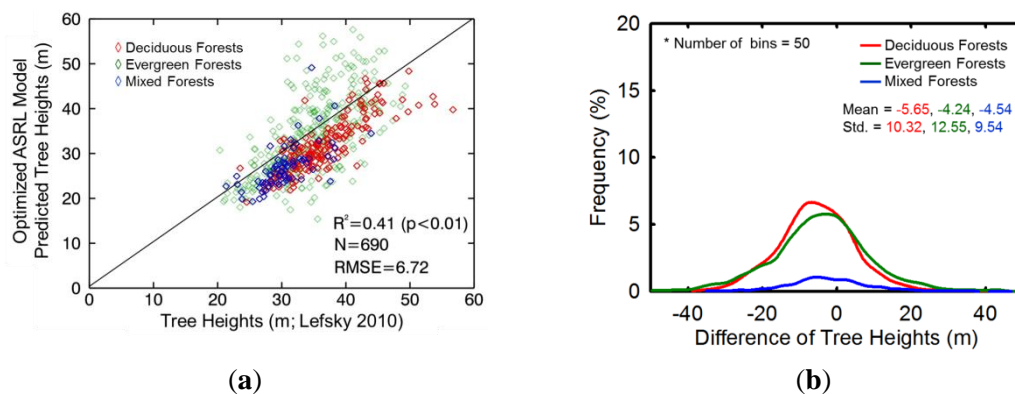


Figure 7(a) depicts a scenario where  $H_{opt\ ASRL}$  is relatively higher in the northwestern and northeastern forested regions as compared to  $H_{Simard}$ . At the scale of climatic zones (Figure 7(b)), the optimized ASRL model predictions are moderately correlated to height values derived by Simard *et al.* [1] ( $R^2 = 0.45$ ;  $RMSE = 8.01$  m;  $P < 0.01$ ). Average values of  $H_{opt\ ASRL}$  for each of the climatic zones were usually higher. Figure 7c shows that the differences between these two maps are nearly independent of forest type. The differences in height values can likely be attributed to differences in definitions of forests—the map from Simard *et al.* [1] used forested areas corresponding to classes such as mosaic crops, open forest, and saline flooded forests. An added *caveat*, as noted in Simard *et al.* [1], was the inability of their regression tree model to simulate forest heights  $>40$  m.

**Figure 7.** Inter-comparison of tree heights predicted by the optimized ASRL model with forest canopy heights from Simard *et al.* [1]: (a) Spatial map showing differences in tree heights ( $H_{opt ASRL} - H_{Simard}$ ). (b) Comparison at the climatic zone level. (c) Pixel level difference histograms ( $H_{opt ASRL} - H_{Simard}$ ) for the three forest types considered in this study. Number of bins of histograms is 50. Frequencies have been normalized by total grids (frequency %).



**Figure 8.** Inter-comparison of tree heights predicted by the optimized ASRL model with tree heights from Lefsky [2]: (a) Comparison for each of the climatic zones ( $H_{opt ASRL}$  and  $H_{Lefsky}$ ). (b) Pixel level difference histograms ( $H_{opt ASRL} - H_{Lefsky}$ ) for the three forest types considered in this study. Number of bins of histograms is 50. Frequencies have been normalized by total grids (frequency %).



We also compared our forest height map with Lefsky’s [2] original GLAS-based tree heights. Figure 8(a) shows a one-to-one comparison between the average height values obtained from  $H_{opt ASRL}$

and  $H_{Lefsky}$  for each of the climate zones. Overall, there is a moderate correlation ( $R^2 = 0.41$ ; RMSE = 6.72 m;  $P < 0.01$ ) between  $H_{opt\ ASRL}$  and  $H_{Lefsky}$ . Mean values of  $H_{opt\ ASRL}$  are an underestimate. Figure 8b shows the pixel level difference ( $H_{opt\ ASRL} - H_{Lefsky}$ ) histograms for three forest types—deciduous forests show higher differences (mean =  $-5.7$  m; std. = 10.3) followed by the evergreen forests (mean =  $-4.2$  m; std. = 12.6) and mixed forest types (mean =  $-4.5$  m; std. = 9.5). A plausible reason could be that Lefsky [2] applied a different height retrieval procedure (statistical) based on full GLAS waveform extents, while our study used the standard Gaussian decomposition approach.

## 6. Concluding Remarks

An optimization of the Allometric Scaling and Resource Limitations (ASRL) model with Geoscience Laser Altimeter System (GLAS) waveform data was performed to generate a spatially continuous map of tree heights over the continental USA (CONUS) at 1 km resolution. The optimization is designed to minimize differences between actual heights (based on GLAS waveforms) and potential tree heights predicted by the ASRL model. This study covered all forested lands with over 50% tree cover. These were categorized into 841 climatic zones based on forest types (deciduous, evergreen, and mixed forests), fixed intervals of annual total precipitation (30 mm) and annual average temperature ( $2\ ^\circ\text{C}$ ). The optimization procedure simultaneously adjusted three model parameters (area of single leaf,  $\alpha$ ; exponent for canopy radius,  $\eta$ ; and root absorption efficiency,  $\gamma$ ) in each of the climatic zones.

After testing for correctly implementing the optimization technique, tree heights predicted by the optimized model were first evaluated using a two-fold cross validation approach. Regression analysis was used to assess the correlation between predictions of tree heights by the optimized model ( $H_{opt\ ASRL\ training}$ ) and test GLAS tree heights ( $H_{GLAS\ test}$ ) in all climatic zones. Mean values of  $H_{opt\ ASRL}$  explained 59% of the variability in  $H_{GLAS\ test}$  mean estimates in each of the climatic zones and, on average, showed an estimation error of 3.31 units of height. A similar evaluation of the optimized ASRL model was performed at FLUXNET sites—this is detailed in the second of this multi-article series [25]. A comparison at the pixel level to quantify the skewness between  $H_{opt\ ASRL\ training}$  (mean = 30.8 m; standard deviation = 10.7) and  $H_{GLAS}$  (mean = 30.6; std. = 8.4) was performed. Predicted tree heights by the optimized model agreed better with GLAS tree heights (mean =  $-0.6$  m; std. = 12.9) in comparison to the estimates from the unoptimized ASRL model. However, the optimized ASRL model still poorly predicted tree heights over the Pacific Northwestern Mountains of California and Oregon.

Second, tree height predictions by the optimized ASRL model were compared with available forest height products derived independently but from the GLAS data—Simard *et al.* [1] ( $H_{Simard}$ ) and Lefsky [2] ( $H_{Lefsky}$ ). The results indicate moderate correlation between optimized ASRL model predicted heights and forest heights from Simard *et al.* [1] and Lefsky [2] for all climatic zones ( $R^2 = 0.45$  and RMSE = 8.01 m for  $H_{Simard}$ ;  $R^2 = 0.41$  and RMSE = 6.72 m for  $H_{Lefsky}$ ).  $H_{opt\ ASRL}$  was an overestimate compared to  $H_{Simard}$  and an underestimate compared to  $H_{Lefsky}$  and with significant skewness at the individual pixel level—these discrepancies can be attributed due to different definitions of heights and forested lands between these studies and certain inherent limitations of the various approaches.

Predictions of tree heights by the ASRL model were clearly improved by the optimization technique reported in this article. The optimization successfully compensated for certain limitations of the original ASRL model, which did not account for effects related to spatio-temporal variability in climatic-regimes and forest types. The results demonstrate the potential for a more generic applicability of the ASRL model for estimation of tree heights. Nevertheless, the optimized ASRL model still yields ambiguous results over complex terrains, possibly due to uncertainties in input climatic data and topographic effects in the GLAS waveform data. The optimization methodology reported in this article has certain limitations: e.g., (a) a limited number of scaling parameters ( $\alpha$ ,  $\eta$ , and  $\gamma$ ) were explored in the model optimization, (b) stand age was not directly considered in the optimization, (c) soil conditions were neglected in the optimization and (d) we assumed that allometric scaling laws at individual tree level were applicable at larger scales. Also, our analysis could not take into account the uncertainties derived from resampling and reprojection of maps and data at different scales and projections. Alleviation of these limitations should be addressed in future articles in this series.

### Acknowledgments

This study was partially funded by the National Natural Science Foundation of China (Grants No. 40801139 and 41175077), China Scholarship Council and the Fulbright Foundation.

### References

1. Simard, M.; Pinto, N.; Fisher, J.B.; Baccini, A. Mapping forest canopy height globally with spaceborne lidar. *J. Geophys. Res.-Biogeosci.* **2011**, *116*, doi: 10.1029/2011jg001708.
2. Lefsky, M.A. A global forest canopy height map from the Moderate Resolution Imaging Spectroradiometer and the Geoscience Laser Altimeter System. *Geophys. Res. Lett.* **2010**, *37*, doi: 10.1029/2010gl043622.
3. Zhang, G.; Ganguly, S.; Nemani, R.; White, M.; Milesi, C.; Wang, W.; Saatchi, S.; Yu, Y.; Myneni, R.B. A simple parametric estimation of live forest aboveground biomass in California using satellite derived metrics of canopy height and Leaf Area Index. *Geophys. Res. Lett.* **2012**, under review.
4. Saatchi, S.S.; Harris, N.L.; Brown, S.; Lefsky, M.; Mitchard, E.T.A.; Salas, W.; Zutta, B.R.; Buermann, W.; Lewis, S.L.; Hagen, S.; Petrova, S.; White, L.; Silman, M.; Morel, A. Benchmark map of forest carbon stocks in tropical regions across three continents. *Proc. Natl. Acad. Sci. USA* **2011**, *108*, 9899–9904.
5. Chopping, M.; Schaaf, C.B.; Zhao, F.; Wang, Z.S.; Nolin, A.W.; Moisen, G.G.; Martonchik, J.V.; Bull, M. Forest structure and aboveground biomass in the southwestern United States from MODIS and MISR. *Remote Sens. Environ.* **2011**, *115*, 2943–2953.
6. Sun, G.; Ranson, K.J.; Kimes, D.S.; Blair, J.B.; Kovacs, K. Forest vertical structure from GLAS: An evaluation using LVIS and SRTM data. *Remote Sens. Environ.* **2008**, *112*, 107–117.
7. Mitchard, E.T.A.; Saatchi, S.S.; Lewis, S.L.; Feldpausch, T.R.; Gerard, F.F.; Woodhouse, I.H.; Meir, P. Comment on “A first map of tropical Africa’s above-ground biomass derived from satellite imagery”. *Environ. Res. Lett.* **2011**, *6*, doi: 10.1088/1748-9326/6/4/049001.

8. Selkowitz, D.J.; Green, G.; Peterson, B.; Wylie, B. A multi-sensor lidar, multi-spectral and multi-angular approach for mapping canopy height in boreal forest regions. *Remote Sens. Environ.* **2012**, *121*, 458–471.
9. Jung, S.-E.; Kwak, D.-A.; Park, T.; Lee, W.-K.; Yoo, S. Estimating crown variables of individual trees using airborne and terrestrial laser scanners. *Remote Sens.* **2011**, *3*, 2346–2363.
10. Straub, C.; Koch, B. Estimating single tree stem volume of *Pinus sylvestris* using airborne laser scanner and multispectral line scanner data. *Remote Sens.* **2011**, *3*, 929–944.
11. Treuhaft, R.N.; Chapman, B.D.; dos Santos, J.R.; Goncalves, F.G.; Dutra, L.V.; Graca, P.M.L.A.; Drake, J.B. Vegetation profiles in tropical forests from multibaseline interferometric synthetic aperture radar, field, and lidar measurements. *J. Geophys. Res.-Atmos.* **2009**, *114*, doi: 10.1029/2008jd011674.
12. Treuhaft, R.N.; Goncalves, F.G.; Drake, J.B.; Chapman, B.D.; dos Santos, J.R.; Dutra, L.V.; Graca, P.M.L.A.; Purcell, G.H. Biomass estimation in a tropical wet forest using Fourier transforms of profiles from lidar or interferometric SAR. *Geophys. Res. Lett.* **2010**, *37*, doi: 10.1029/2010gl045608.
13. Baccini, A.; Goetz, S.J.; Walker, W.S.; Laporte, N.T.; Sun, M.; Sulla-Menashe, D.; Hackler, J.; Beck, P.S.A.; Dubayah, R.; Friedl, M.A.; Samanta, S.; Houghton, R.A. Estimated carbon dioxide emissions from tropical deforestation improved by carbon-density maps. *Nature Clim. Change* **2012**, *2*, 182–185.
14. Kempes, C.P.; West, G.B.; Crowell, K.; Girvan, M. Predicting maximum tree heights and other traits from allometric scaling and resource limitations. *Plos One* **2011**, *6*, doi: 10.1371/journal.pone.0020551.
15. Kozlowski, J.; Konarzewski, M. Is West, Brown and Enquist's model of allometric scaling mathematically correct and biologically relevant? *Funct. Ecol.* **2004**, *18*, 283–289.
16. Kozlowski, J.; Konarzewski, M. West, Brown and Enquist's model of allometric scaling again: The same questions remain. *Funct. Ecol.* **2005**, *19*, 739–743.
17. Zianis, D. Predicting mean aboveground forest biomass and its associated variance. *Forest Ecol. Manage.* **2008**, *256*, 1400–1407.
18. Etienne, R.S.; Apol, M.E.F.; Olf, H. Demystifying the West, Brown & Enquist model of the allometry of metabolism. *Funct. Ecol.* **2006**, *20*, 394–399.
19. Brown, J.H.; Gillooly, J.F.; Allen, A.P.; Savage, V.M.; West, G.B. Response to forum commentary on “toward a metabolic theory of ecology”. *Ecology* **2004**, *85*, 1818–1821.
20. Brown, J.H.; West, G.B.; Enquist, B.J. Yes, West, Brown and Enquist's model of allometric scaling is both mathematically correct and biologically relevant. *Funct. Ecol.* **2005**, *19*, 735–738.
21. Enquist, B.J.; West, G.B.; Brown, J.H. Extensions and evaluations of a general quantitative theory of forest structure and dynamics. *Proc. Natl. Acad. Sci. USA* **2009**, *106*, 7046–7051.
22. West, G.B.; Enquist, B.J.; Brown, J.H. A general quantitative theory of forest structure and dynamics. *Proc. Natl. Acad. Sci. USA* **2009**, *106*, 7040–7045.
23. Chojnacky, D.C. Allometric Scaling Theory Applied to FIA Biomass Estimation. In *Proceedings of the Third Annual Forest Inventory and Analysis Symposium*; McRoberts, R.E., Reams, G.A., Van Deusen, P.C., Moser, J.W., Eds.; Gen. Tech. Rep. NC-230; North Central Research Station, USDA, Forest Service: St. Paul, MN, USA, 2002; Volume 230, pp. 96–102.

24. Cheng, D.L.; Li, T.; Zhong, Q.L.; Wang, G.X. Scaling relationship between tree respiration rates and biomass. *Biol. Lett.* **2010**, *6*, 715–717.
25. Choi, S.; Ni, S.; Shi, Y.; Ganguly, S.; Zhang, G.; Duong, H.V.; Lefsky, M.A.; Simard, M.; Saatchi, S.S.; Lee, S.; *et al.* Allometric scaling and resource limitations model of tree heights: Part 2. Site based testing of the model. *Remote Sens.* **2013**, *5*, 202–223.
26. ESRI. ArcGIS Desktop 9.2 Help Desk: Resampling Under Data Management. Available online: [http://webhelp.esri.com/arcgisdesktop/9.2/index.cfm?TopicName=resample\\_\(data\\_management\)](http://webhelp.esri.com/arcgisdesktop/9.2/index.cfm?TopicName=resample_(data_management)) (accessed on 12 July 2012).
27. Luo, W.; Taylor, M.C.; Parker, S.R. A comparison of spatial interpolation methods to estimate continuous wind speed surfaces using irregularly distributed data from England and Wales. *Int. J. Climatol.* **2008**, *28*, 947–959.
28. DAYMET. Available online: <http://www.daymet.org/> (accessed on 12 July 2012).
29. World Meteorological Organization (WMO). *Guide to Meteorological Instruments and Methods of Observation, Appendix 4B*; WMO-No. 8 (CIMO Guide); WMO: Geneva, Switzerland, 2008.
30. North American Regional Reanalysis (NARR). Available online: <http://www.emc.ncep.noaa.gov/mmb/rrean/> (accessed on 12 July 2012).
31. Gesch, D.; Evans, G.; Mauck, J.; Hutchinson, J.; Carswell, W.J. *The National Map—Elevation: U.S. Geological Survey Fact Sheet 2009-3053*; 2009; p.4.
32. Yuan, H.; Dai, Y.J.; Xiao, Z.Q.; Ji, D.Y.; Wei, S.G. Reprocessing the MODIS Leaf Area Index products for land surface and climate modelling. *Remote Sens. Environ.* **2011**, *115*, 1171–1187.
33. Fry, J.A.; Xian, G.; Jin, S.M.; Dewitz, J.A.; Homer, C.G.; Yang, L.M.; Barnes, C.A.; Herold, N.D.; Wickham, J.D. Completion of the 2006 National Land Cover Database for the Conterminous United States. *Photogramm. Eng. Remote Sensing* **2011**, *77*, 859–864.
34. Hansen, M.C.; DeFries, R.S.; Townshend, J.R.G.; Carroll, M.; Dimiceli, C.; Sohlberg, R.A. Global percent tree cover at a spatial resolution of 500 meters: First results of the MODIS Vegetation Continuous Fields Algorithm. *Earth Interact.* **2003**, *7*, 1–10.
35. Zwally, H.J.; Schutz, B.; Abdalati, W.; Abshire, J.; Bentley, C.; Brenner, A.; Bufton, J.; Dezio, J.; Hancock, D.; Harding, D.; *et al.* ICESat’s laser measurements of polar ice, atmosphere, ocean, and land. *J. Geodyn.* **2002**, *34*, 405–445.
36. Abshire, J.B.; Sun, X.L.; Riris, H.; Sirota, J.M.; McGarry, J.F.; Palm, S.; Yi, D.H.; Liiva, P. Geoscience Laser Altimeter System (GLAS) on the ICESat mission: On-orbit measurement performance. *Geophys. Res. Lett.* **2005**, *32*, doi: 10.1029/2005gl024028.
37. Brenner, A.C.; Bentley, C.R.; Csatho, B.M.; Harding, D.J.; Hofton, M.A.; Minster, J.; Roberts, L.; Saba, J.L.; Schutz, R.; Thomas, R.H.; Yi, D.; Zwally, H.J. *Derivation of Range and Range Distributions from Laser Pulse Waveform Analysis for Surface Elevations, Roughness, Slope, and Vegetation Heights*; Algorithm Theoretical Basis Document Version 4.1; NASA Goddard Space Flight Center: Greenbelt, MD, USA, 2003; p. 12.
38. Neuenschwander, A.L.; Urban, T.J.; Gutierrez, R.; Schutz, B.E. Characterization of ICESat/GLAS waveforms over terrestrial ecosystems: Implications for vegetation mapping. *J. Geophys. Res.-Biogeosci.* **2008**, *113*, doi: 10.1029/2007jg000557.
39. Gong, P.; Li, Z.; Huang, H.B.; Sun, G.Q.; Wang, L. ICESat GLAS data for urban environment monitoring. *IEEE Trans. Geosci. Remote Sens.* **2011**, *49*, 1158–1172.

40. Lee, S.; Ni-Meister, W.; Yang, W.Z.; Chen, Q. Physically based vertical vegetation structure retrieval from ICESat data: Validation using LVIS in White Mountain National Forest, New Hampshire, USA. *Remote Sens. Environ.* **2011**, *115*, 2776–2785.
41. Chen, Q. Retrieving vegetation height of forests and woodlands over mountainous areas in the Pacific Coast region using satellite laser altimetry. *Remote Sens. Environ.* **2010**, *114*, 1610–1627.
42. Lefsky, M.A.; Keller, M.; Pang, Y.; de Camargo, P.B.; Hunter, M.O. Revised method for forest canopy height estimation from Geoscience Laser Altimeter System waveforms. *J. Appl. Remote Sens.* **2007**, *1*, doi: 10.1117/1.2795724.
43. Duncanson, L.I.; Niemann, K.O.; Wulder, M.A. Estimating forest canopy height and terrain relief from GLAS waveform metrics. *Remote Sens. Environ.* **2010**, *114*, 138–154.
44. Pang, Y.; Lefsky, M.; Sun, G.Q.; Ranson, J. Impact of footprint diameter and off-nadir pointing on the precision of canopy height estimates from spaceborne lidar. *Remote Sens. Environ.* **2011**, *115*, 2798–2809.
45. Harding, D.J.; Carabajal, C.C. ICESat waveform measurements of within-footprint topographic relief and vegetation vertical structure. *Geophys. Res. Lett.* **2005**, *32*, doi: 10.1029/2005gl023471.
46. Neuenschwander, A.L. Evaluation of waveform deconvolution and decomposition retrieval algorithms for ICESat/GLAS data. *Can. J. Remote Sens.* **2008**, *34*, S240–S246.
47. Rosette, J.A.B.; North, P.R.J.; Suarez, J.C.; Los, S.O. Uncertainty within satellite LiDAR estimations of vegetation and topography. *Int. J. Remote Sens.* **2010**, *31*, 1325–1342.
48. Lagerloef, G.S.E.; Bernstein, R.L. Empirical orthogonal function-analysis of Advanced Very High-Resolution Radiometer surface-temperature patterns in Santa-Barbara Channel. *J. Geophys. Res.-Oceans* **1988**, *93*, 6863–6873.
49. Choi, S.; Lee, W.K.; Son, Y.; Yoo, S.; Lim, J.H. Changes in the distribution of South Korean forest vegetation simulated using thermal gradient indices. *Sci. China Life Sci.* **2010**, *53*, 784–797.
50. Powell, M.J.D. An efficient method for finding the minimum of a function of several variables without calculating derivatives. *Comput. J.* **1964**, *7*, 155–162.
51. Press, W.H.; Teukolsky, S.A.; Vetterling, W.T.; Flannery, B.P. Minimization or Maximization of Functions. In *Numerical Recipes in FORTRAN: The Art of Scientific Computing*, 2nd ed.; Chapter 10; Cambridge University Press: Cambridge, UK/New York, NY, USA, 1992; pp. 394–445.
52. Kuusk, A.; Nilson, T. A directional multispectral forest reflectance model. *Remote Sens. Environ.* **2000**, *72*, 244–252.
53. TRY. Plant Trait Database. Available online: <http://www.try-db.org/TryWeb/Home.php> (accessed on 12 July 2012).
54. Kattge, J.; Diaz, S.; Lavorel, S.; Prentice, C.; Leadley, P.; Bonisch, G.; Garnier, E.; Westoby, M.; Reich, P.B.; Wright, I.J.; et al. TRY—A global database of plant traits. *Glob. Change Biol.* **2011**, *17*, 2905–2935.
55. West, G.B.; Brown, J.H.; Enquist, B.J. A general model for the structure and allometry of plant vascular systems. *Nature* **1999**, *400*, 664–667.
56. Ridler, M.E.; Sandholt, I.; Butts, M.; Lerer, S.; Mougín, E.; Timouk, F.; Kergoat, L.; Madsen, H. Calibrating a soil–vegetation–atmosphere transfer model with remote sensing estimates of surface temperature and soil surface moisture in a semi arid environment. *J. Hydrol.* **2012**, *436–437*, 1–12.

57. Gholz, H.L. Environmental limits on aboveground net primary production, leaf area, and biomass in vegetation zones of the Pacific Northwest. *Ecology* **1982**, *63*, 469–481.
58. Smith, T.M.; Shugart, H.H.; Bonan, G.B.; Smith, J.B. Modeling the potential response of vegetation to global climate change. *Adv. Ecol. Res.* **1992**, *22*, 93–116.
59. O'Brien, S.T.; Hubbell, S.P.; Spiro, P.; Condit, R.; Foster, R.B. Diameter, height, crown, and age relationships in 8 neotropical tree species. *Ecology* **1995**, *76*, 1926–1939.
60. Shugart, H.H.; Saatchi, S.; Hall, F.G. Importance of structure and its measurement in quantifying function of forest ecosystems. *J. Geophys. Res.-Biogeo.* **2010**, *115*, doi: 10.1029/2009jg000993.
61. Ryan, M.G.; Yoder, B.J. Hydraulic limits to tree height and tree growth. *Bioscience* **1997**, *47*, 235–242.
62. Pan, Y.; Chen, J.M.; Birdsey, R.; McCullough, K.; He, L.; Deng, F. Age structure and disturbance legacy of North American forests. *Biogeosciences* **2011**, *8*, 715–732.
63. Nadeau, C.; Bengio, Y. Inference for the generalization error. *Mach. Learn.* **2003**, *52*, 239–281.
64. Wu, J.; Jelinski, D.E.; Luck, M.; Tueller, P.T. Multiscale Analysis of Landscape Heterogeneity: Scale Variance and Pattern Metrics. *Geogr. Inf. Sci.* **2000**, *6*, 6–19.
65. Wu, H.; Li, Z.L. Scale issues in remote sensing: A review on analysis, processing and modeling. *Sensors* **2009**, *9*, 1768–1793.
66. Seong, J.C. Modelling the accuracy of image data reprojection. *Int. J. Remote Sens.* **2003**, *24*, 2309–2321.
67. Pandey, G.R.; Cayan, D.R.; Dettinger, M.D.; Georgakakos, K.P. A hybrid orographic plus statistical model for downscaling daily precipitation in northern California. *J. Hydrometeorol.* **2000**, *1*, 491–506.
68. Lundquist, J.D.; Cayan, D.R. Surface temperature patterns in complex terrain: Daily variations and long-term change in the central Sierra Nevada, California. *J. Geophys. Res.-Atmos.* **2007**, *112*, doi: 10.1029/2006jd007561.
69. Parkhurst, D.F.; Loucks, O.L. Optimal leaf size in relation to environment. *J. Ecol.* **1972**, *60*, 505–537.
70. Grier, C.C.; Running, S.W. Leaf area of mature Northwestern Coniferous Forests—Relation to site water-balance. *Ecology* **1977**, *58*, 893–899.
71. Westoby, M.; Falster, D.S.; Moles, A.T.; Vesk, P.A.; Wright, I.J. Plant ecological strategies: Some leading dimensions of variation between species. *Annu. Rev. Ecol. Syst.* **2002**, *33*, 125–159.
72. Golluscio, R.A.; Oesterheld, M. Water use efficiency of twenty-five co-existing Patagonian species growing under different soil water availability. *Oecologia* **2007**, *154*, 207–217.
73. Goldstein, G.; Rada, F.; Rundel, P.; Azocar, A.; Orozco, A. Gas-exchange and water relations of evergreen and deciduous tropical savanna trees. *Ann. Sci. Forest.* **1989**, *46*, S448–S453.
74. Medina, E.; Francisco, M. Photosynthesis and water relations of savanna tree species differing in leaf phenology. *Tree Physiol.* **1994**, *14*, 1367–1381.

Supplementary Information

## Allometric Scaling and Resource Limitations Model of Tree Heights: Part 1. Model Optimization and Testing over Continental USA. *Remote Sens.* 2013, 5, 284–306

**Yuli Shi**<sup>1,2,†</sup>, **Sungho Choi**<sup>2,†,\*</sup>, **Xiliang Ni**<sup>2,3</sup>, **Sangram Ganguly**<sup>4</sup>, **Gong Zhang**<sup>5</sup>, **Hieu V. Duong**<sup>6</sup>, **Michael A. Lefsky**<sup>6</sup>, **Marc Simard**<sup>7</sup>, **Sassan S. Saatchi**<sup>7</sup>, **Shihyan Lee**<sup>8</sup>, **Wenge Ni-Meister**<sup>8</sup>, **Shilong Piao**<sup>9</sup>, **Chunxiang Cao**<sup>3</sup>, **Ramakrishna R. Nemani**<sup>10</sup> and **Ranga B. Myneni**<sup>2</sup>

<sup>1</sup> School of Remote Sensing, Nanjing University of Information Science and Technology, Nanjing 210044, China; E-Mail: ylshi.nuist@gmail.com

<sup>2</sup> Department of Earth and Environment, Boston University, 675 Commonwealth Avenue, Boston, MA 02215, USA; E-Mail: ranga.myneni@gmail.com

<sup>3</sup> State Key Laboratory of Remote Sensing Sciences, Institute of Remote Sensing Applications, Chinese Academy of Sciences, Beijing 100101, China; E-Mails: nixl@irsa.ac.cn (X.N.); cao413@irsa.ac.cn (C.C.)

<sup>4</sup> Bay Area Environmental Research Institute (BAERI)/NASA Ames Research Center, Moffett Field, CA 94035, USA; E-Mail: sangramganguly@gmail.com

<sup>5</sup> Department of Watershed Science, Utah State University, Logan, UT 84322, USA; E-Mail: gongzhang07@gmail.com

<sup>6</sup> Center for Ecological Analysis of Lidar, Natural Resource Ecology Laboratory, Colorado State University, Fort Collins, CO 80523, USA; E-Mails: dr.hieu.duong@gmail.com (H.D.); lefsky@cnr.colostate.edu (M.L.)

<sup>7</sup> Jet Propulsion Laboratory, California Institute of Technology, 4800 Oak Grove Dr., Pasadena, CA 91109, USA; E-Mails: marc.simard@jpl.nasa.gov (M.S.); saatchi@jpl.nasa.gov (S.S.)

<sup>8</sup> Department of Geography, Hunter College of CUNY, New York, NY 10065, USA; E-Mails: shihyanlee@yahoo.com (S.L.); Wenge.Ni-Meister@hunter.cuny.edu (W.N.)

<sup>9</sup> College of Urban and Environmental Sciences and Sino-French Institute for Earth System Science, Peking University, Beijing 100871, China; E-Mail: slpiao@pku.edu.cn

<sup>10</sup> Biospheric Science Branch, NASA Ames Research Center, Moffett Field, CA 94035, USA; E-Mail: rama.nemani@nasa.gov

† These authors contributed equally to this work.

\* Author to whom correspondence should be addressed; E-Mail: schoi@bu.edu; Tel.: +1-617-353-8846; Fax: +1-617-353-8846.

## List of Abbreviations

ASRL	Allometric Scaling and Resource Limitations
DEM	Digital Elevation Model
GLA14	GLAS Level-2 Land Surface Altimetry
GLAS	Geoscience Laser Altimeter System
ICESat	Ice, Cloud, and land Elevation Satellite
IDW	Inverse Distance Weighting
LAI	Leaf Area Index
LVIS	Laser Vegetation Imaging Sensor
MODIS	Moderate Resolution Imaging Spectroradiometer
NARR	North American Regional Reanalysis
NDVI	Normalized Vegetation Difference Vegetation Index
NED	National Elevation Dataset
NLCD	National Land Cover Database
RMSE	Root Mean Square Error
TSF	Temporal Spatial Filter
VCF	Vegetation Continuous Fields
WMO	World Meteorology Organization

## S1. Data

### S1.1. Annual Average Relative Humidity

Annual average temperature and annual average vapor pressure from DAYMET data were converted to annual average relative humidity ( $\Phi$ ) using a formula provided by World Meteorological Organization (WMO) [1] (Equation (S1)).

$$\Phi = \frac{e_w}{e_w^*} \times 100 \quad (S1)$$

$$e_w^* = 6.112e^{17.62T/(243.12+T)}$$

Here  $e_w$  is vapor pressure (hPa),  $e_w^*$  is saturated vapor pressure (hPa) and  $T$  is air temperature ( $^{\circ}\text{C}$ ).

### S1.2. Growing Season Average Leaf Area Index

An input to the ASRL model is the growing season average Leaf Area Index (LAI). This was derived from a refined version of the standard Moderate Resolution Imaging Spectroradiometer (MODIS) LAI product [2]. As documented in Yuan *et al.* [3], the standard MODIS LAI product was post-processed using a two-step integrated approach: (a) a modified version of a temporal spatial filter (TSF) was applied [4,5] that replaced lower quality data to an equivalent best case scenario (gap filled data) based on quality control (QC) layers and (b) the final post-processing of the LAI product was performed using the TIMESAT Savitzky-Golay (SG) filter [6]. The 8-day composites of the post-

processed MODIS LAI product from 2003 to 2008 (June to September; approximate growing season) were used to evaluate growing season average LAI data based on Equation (S2):

$$\overline{LAI}_{gs\_avg.} = \frac{\sum_{i=1}^n \sum_{j=1}^m \overline{LAI}_{8-day,i,j}}{m \times n} \quad (S2)$$

Here  $\overline{LAI}_{gs\_avg.}$  is the approximate growing season average LAI (June to September months from years 2003 to 2006),  $\overline{LAI}_{8-day,i,j}$  is the 8-day LAI product for  $i^{\text{th}}$  week ( $m = 16$ ) of  $j^{\text{th}}$  year ( $n = 4$ ).

## S2. Figures S1–S5

**Figure S1.** Distribution of GLAS heights over the continental USA. We applied a Gaussian decomposition approach of Lee *et al.* [7] using the signal begin range increment (*SigBegOff*) and the last peak of Gaussians (*gpCntRntOff* 1). The potential bias due to topographic conditions has been rectified [7]. This GLAS height metric is well correlated to field-measured and airborne lidar-derived tree heights [8]. Each raster (size 1 km) is not visible at a continental scale. So, we implemented point symbols corresponding to each pixel for better presenting of GLAS-derived tree heights in this figure.

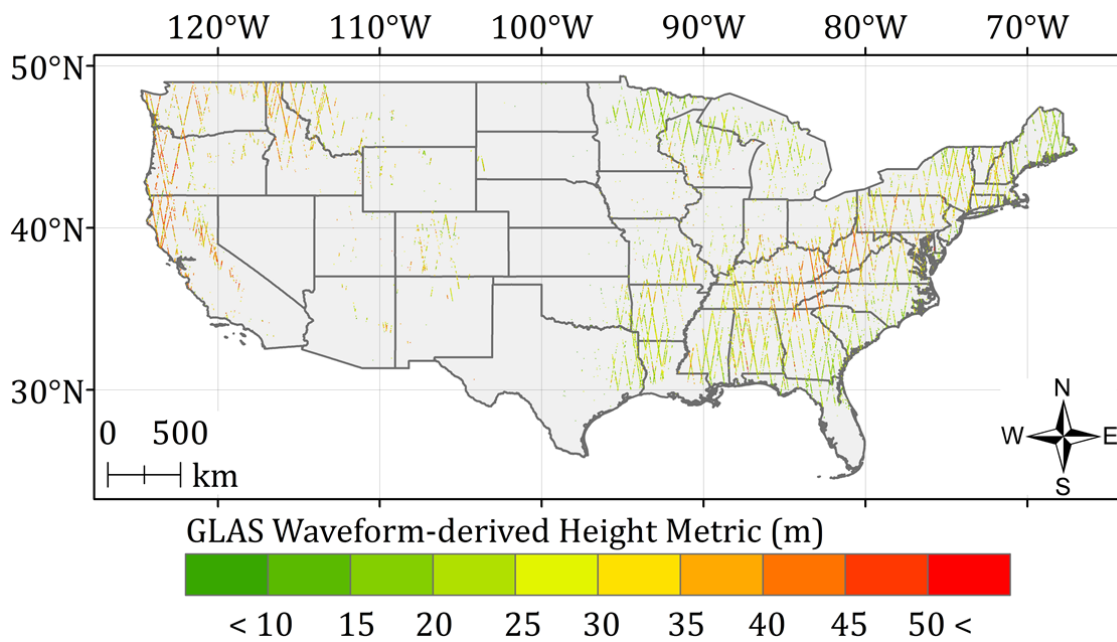


**Figure S2.** Distribution of climatic zones over the empirical orthogonal panel of annual total precipitation and annual average temperature. Climatic zones were defined based on three forest types (deciduous, evergreen and mixed forests) and fixed intervals of precipitation (30 mm) and temperature (2 °C) over the continental USA. The study area was thus confined to 841 climatic zones.

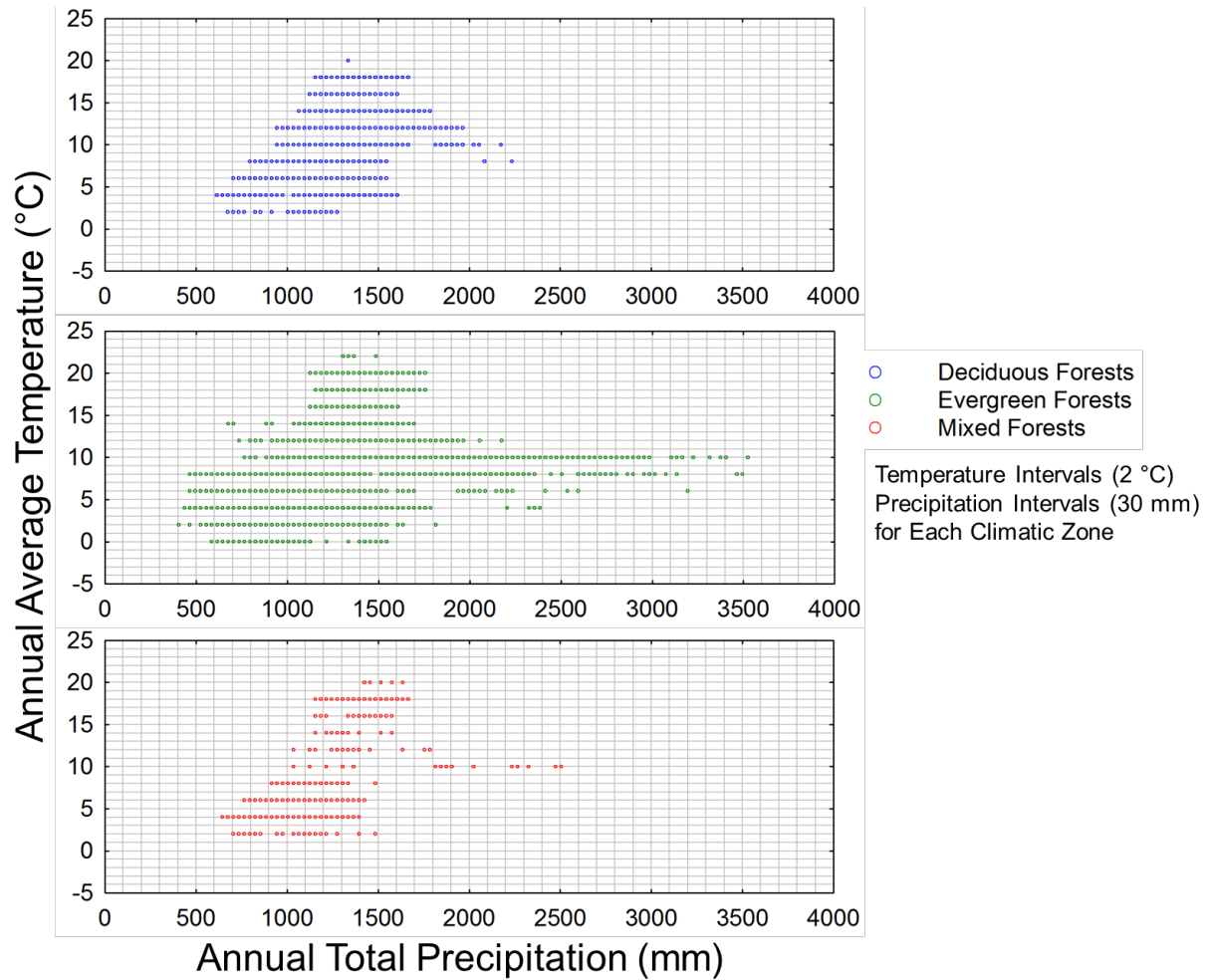


**Figure S3.** Spatial distribution of ASRL model prediction errors at pixel level. **(a)** Without optimization ( $H_{potential\ ASRL} - H_{GLAS}$ ). **(b)** After optimization ( $H_{opt\ ASRL} - H_{GLAS}$ ). See Figure S4 for corresponding histograms.

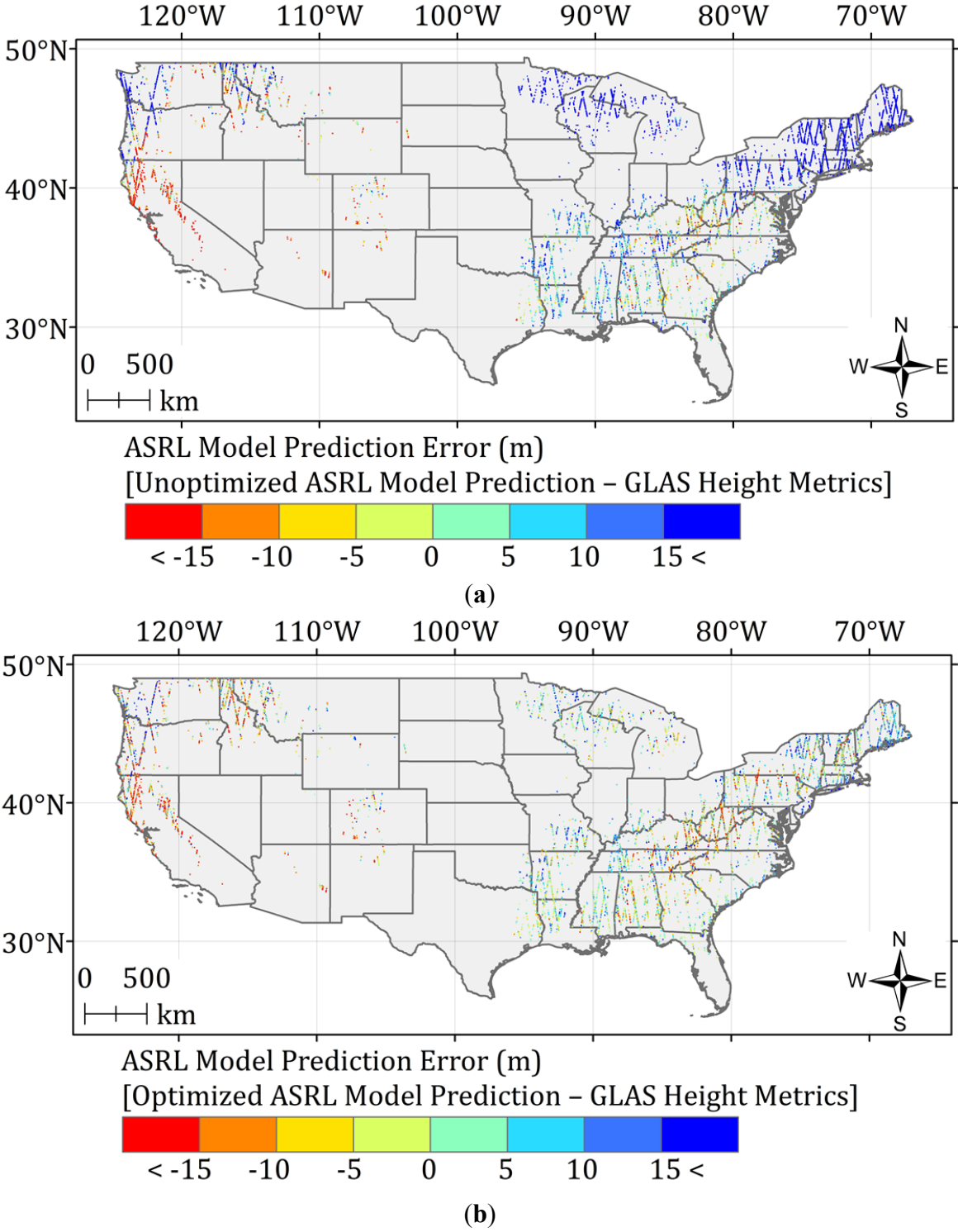


**Figure S4.** Histograms of ASRL model prediction errors at pixel level. **(a)** Without optimization ( $H_{potential\ ASRL} - H_{GLAS}$ ). **(b)** After optimization ( $H_{opt\ ASRL} - H_{GLAS}$ ).

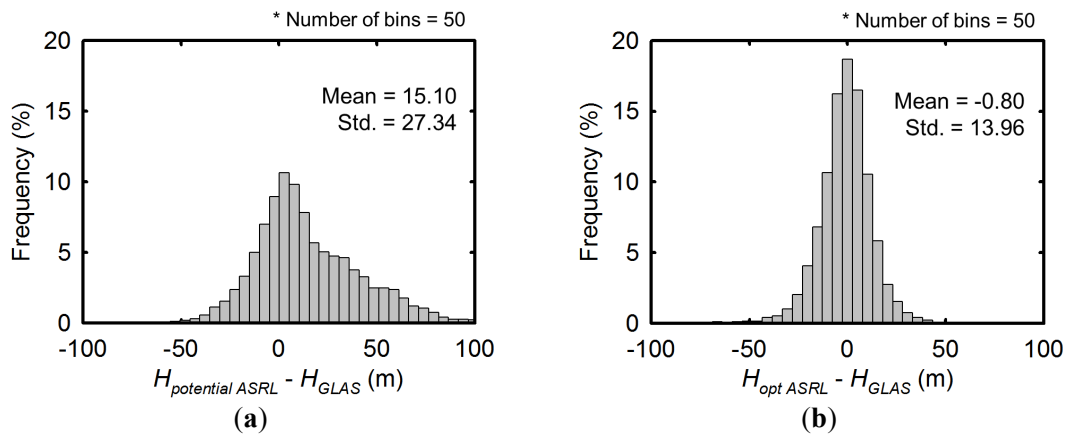
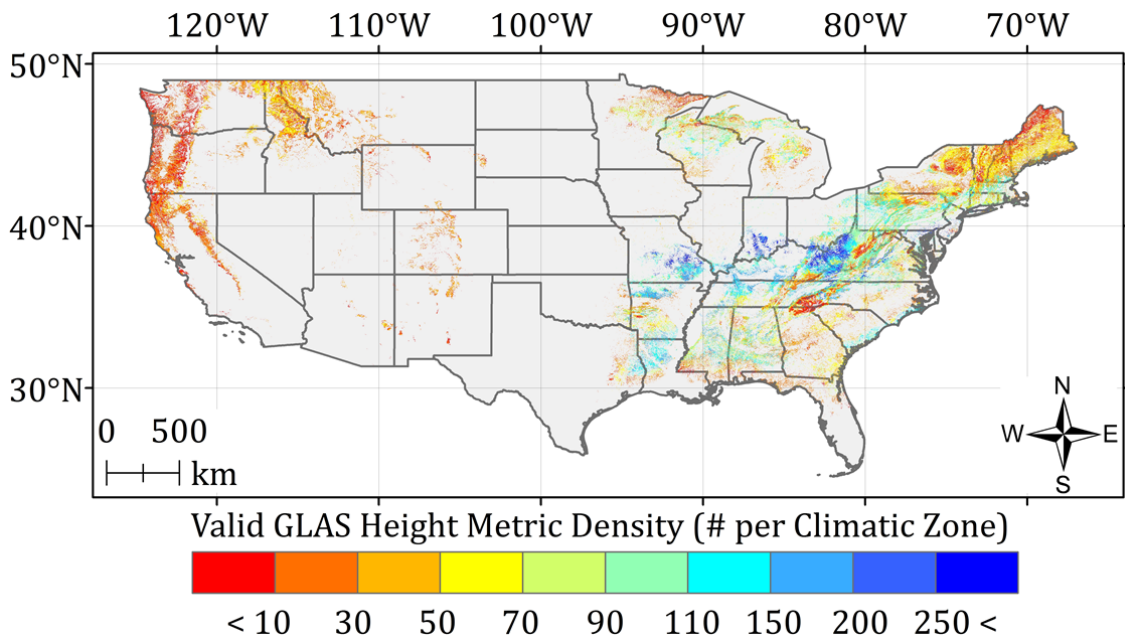


**Figure S5.** Number of valid GLAS data in each of the climatic zones considered in this study. Valid GLAS data density is relatively lower in the Northeastern Appalachian and Pacific Northwestern forest corridors.



## References

1. World Meteorological Organization (WMO). *Guide to Meteorological Instruments and Methods of Observation, Appendix 4B, WMO-No. 8 (CIMO Guide)*; WMO: Geneva, Switzerland, 2008.
2. Land-Atmosphere Interaction Research Group at Beijing Normal University (BNU). LAI Data Sets for Land Surface and Climate Modeling. Available online: <http://globalchange.bnu.edu.cn/research/lai/> (accessed on 12 July 2012).
3. Yuan, H.; Dai, Y.J.; Xiao, Z.Q.; Ji, D.Y.; Wei, S.G. Reprocessing the MODIS Leaf Area Index products for land surface and climate modelling. *Remote Sens. Environ.* **2011**, *115*, 1171–1187.

4. Fang, H.L.; Liang, S.L.; Kim, H.Y.; Townshend, J.R.; Schaaf, C.L.; Strahler, A.H.; Dickinson, R.E. Developing a spatially continuous 1 km surface albedo data set over North America from Terra MODIS products. *J. Geophys. Res.-Atmos.* **2007**, *112*, doi: 10.1029/2006JD008377.
5. Fang, H.L.; Liang, S.L.; Townshend, J.R.; Dickinson, R.E. Spatially and temporally continuous LAI data sets based on an integrated filtering method: Examples from North America. *Remote Sens. Environ.* **2008**, *112*, 75–93.
6. Jonsson, P.; Eklundh, L. TIMESAT—A program for analyzing time-series of satellite sensor data. *Comput. Geosci-UK.* **2004**, *30*, 833–845.
7. Lee, S.; Ni-Meister, W.; Yang, W.Z.; Chen, Q. Physically based vertical vegetation structure retrieval from ICESat data: Validation using LVIS in White Mountain National Forest, New Hampshire, USA. *Remote Sens. Environ.* **2011**, *115*, 2776–2785.
8. Choi, S.; Ni, S.; Shi, Y.; Ganguly, S.; Zhang, G.; Duong, H.V.; Lefsky, M.A.; Simard, M.; Saatchi, S.S.; Lee, S.; *et al.* Allometric scaling and resource limitations model of tree heights: Part 2. Site based testing of the model. *Remote Sens.* **2013**, *5*, 202–223.

© 2013 by the authors; licensee MDPI, Basel, Switzerland. This article is an open access article distributed under the terms and conditions of the Creative Commons Attribution license (<http://creativecommons.org/licenses/by/3.0/>).